

Reasoning aligns language models to human cognition

Gonçalo Guiomar ^{*1 2} Elia Torre ^{*3 2}
 Pehuen Moure ² Victoria Shavina ² Mario Julianelli ⁴ Shih-Chii Liu ² Valerio Mante ^{3 2}

Abstract

Do language models make decisions under uncertainty like humans do? And if so, what role does *chain-of-thought* (CoT) reasoning play in the underlying decision process? We answer this question by introducing an *active probabilistic reasoning* task that cleanly separates *sampling* (actively acquiring evidence) from *inference* (integrating evidence towards a decision). Benchmarking humans and a broad set of contemporary LLMs against near-optimal reference policies reveals a consistent pattern: extended reasoning is the key determinant of strong performance, driving large gains in inference and producing belief trajectories that become strikingly human-like, while yielding only modest improvements in active sampling. To explain these differences, we fit a mechanistic model that captures systematic deviations from optimal behavior via four interpretable latent variables, placing humans and models in a shared low-dimensional *cognitive space*. The resulting fits show how CoT shifts models toward human-like regimes of evidence accumulation and belief-to-choice mapping, tightening alignment in inference while leaving a persistent gap in information acquisition.

1. Introduction

Chain-of-thought (CoT) prompting can substantially improve LLM performance on challenging benchmarks, often reaching near-human accuracy, by eliciting intermediate, step-by-step reasoning (Nye et al., 2021; Reynolds and McDonell, 2021; Wei et al., 2022; Kojima et al., 2022; Wang et al., 2022a; Chen et al., 2025a; Jaech et al., 2024; Guo et al., 2025a; El-Kishky et al., 2025). However, it remains

^{*}Equal contribution ¹ETH AI Center, Zürich, Switzerland
²Institute for Neuroinformatics, University of Zürich & ETH Zürich, Switzerland ³ETH Zürich, Switzerland ⁴University College London, London, United Kingdom. Correspondence to: Gonçalo Guiomar & Elia Torre <goncalo.guiomar@ai.ethz.ch & elia.torre@uzh.ch>.

unclear *why CoT* helps and *how* these reasoning traces relate to the computations that actually produce the answer. Indeed, CoT narratives can be unreliable and can diverge from the model’s internal processes, implying that they do not necessarily describe the true algorithm that a model applied in solving a task (Turpin et al., 2023; Lanham et al., 2023; Barez et al., 2025; Chen et al., 2025b; Arcuschin et al., 2025).

More generally, algorithmic-level descriptions that capture the abstract representations and processes explaining the behavior of LLMs are arguably missing for most current benchmarks (Moskvichev et al., 2023). Yet, a long line of work in cognitive neuroscience suggests that such descriptions could be critically important for any attempts to link a behavior to specific parameters and activations in the underlying circuits (Marr, 2010; Lengyel, 2024). Making explicit the algorithms and representations that lead to a particular behavior can yield *interpretable latent variables* that are often more directly tied to activations than the observable behavior, and thus help bridge what in most tasks is a wide conceptual gap between behavior and the underlying very complex, high-dimensional activations (Lengyel, 2024; Ku et al., 2025).

Such algorithmic descriptions are also needed to evaluate human–LLM alignment when LLMs are treated as candidate *models of human cognition*, and to assess how CoT shapes that alignment. Fine-tuning on human feedback and behavioral datasets can make LLMs reproduce human-like choices and signatures of classic cognitive models (Lake et al., 2017; Peterson et al., 2021; Wei et al., 2021; Bai et al., 2022; Ouyang et al., 2022; Binz and Schulz, 2023a; Momentè et al., 2025; Binz et al., 2025). Yet, performance and behavioral similarity alone may not be sufficient to conclude that LLMs rely on the same latent computations and decision strategies as humans.

In this work, we take inspiration from cognitive neuroscience by developing a behavioral task that isolates two core elements of decision-making under uncertainty: *sampling* and *inference*. Despite its simple structure, our task is demanding, making it a sensitive benchmark for both humans and frontier LLMs. Crucially, behavior in our task can be explained in terms of the dynamics of a few, interpretable

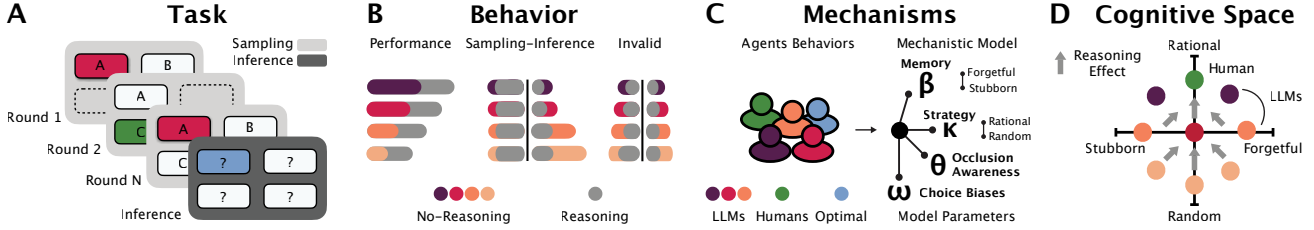


Figure 1. From task performance to latent cognitive variables. **A: Task.** We introduce an *active probabilistic reasoning* task in which agents sequentially sample from up to four buttons (A–D), each revealing a binary outcome (RED/GREEN). One button is biased toward RED, while the others are unbiased. During N sampling rounds, agents actively choose what evidence to sample among the buttons available on a given round. In a final *inference* round, agents indicate which button they believe is biased. An equivalent text-based version is used for LLMs (Appendix B). **B: Behavior.** We compare human and LLM behavior by quantifying overall performance, sampling/inference quality, and invalid choices. These metrics reveal a broad spectrum of performance, with extended *chain-of-thought* reasoning improving overall success via enhanced inference, while gains in sampling remain limited. **C: Mechanisms.** To move beyond behavioral scores, we fit a mechanistic model that captures deviations from optimal Bayesian inference using four interpretable latent variables: **Memory** (β), **Strategy** (κ), **Choice Bias** (ω), and **Occlusion Awareness** (θ). **D: Cognitive Space.** These latent variables define a shared low-dimensional cognitive space in which humans and models can be positioned. Reasoning shifts LLMs toward human-like inference strategies, and tightens, but does not fully close, the gap in sampling strategies.

latent variables, which capture the agents’ strategies and how they are shaped by *CoT*. Concretely, we make the three following contributions:

- We introduce an *active probabilistic reasoning task* that disentangles *sampling* (evidence acquisition) from *inference* (evidence integration) and is well-suited for algorithmic, process-level analysis of behavior (Section 3, Fig. 1A).
- We evaluate a broad set of LLMs and human participants under identical instructions, and use near-optimal reference policies to assess *sampling* and *inference quality* separately. These analyses reveal a broad spectrum of performance with several models reaching human-level. Some models exceed humans in inference quality, but consistently under-perform in sampling quality (Sections 4, 5, 6, Fig. 1B; Fig. 2).
- We develop a mechanistic model that captures how agents sample evidence and update their beliefs in our task. The model places humans and LLMs in a shared *cognitive space* of four latent cognitive variables: **Memory**- β , **Strategy**- κ , **Choice Bias**- ω , **Occlusion Awareness**- θ . Fits of this model reveal that *chain-of-thought* reasoning improves LLM performance by shifting their sampling and inference strategies closer to those of humans (Section 7, 8; Fig. 1C–D; Fig. 3 and 4).

2. Related Work

In recent literature, LLMs are increasingly studied as generalist decision-making agents that act in dynamic environments and adapt via *in-context learning* (ICL) and *in-context reinforcement learning* (ICRL) (Brown et al., 2020; Yao et al., 2022; Laskin et al., 2022; Shinn et al., 2023; Liu et al., 2023a,b; Dong et al., 2024; Moeini et al., 2025). The same domain-general competence motivates a comple-

mentary line of work that treats LLMs not only as capable agents, but as *candidate models* of human cognition. Since a single fixed model can be evaluated across diverse tasks, it provides a substrate for which observable behaviors could potentially be precisely linked to internal representations (Schrimpf et al., 2021; Frank, 2023; Binz and Schulz, 2023b; Aher et al., 2023; Zhao et al., 2025; Loo et al., 2026). These two lines of work intersect in sequential decision-making settings, such as classical multi-armed bandits (MABs) and their variants (Slivkins, 2019; Lattimore and Szepesvári, 2020). In these settings, LLMs can leverage bandit feedback to improve their choices in-context (Lee et al., 2023; Coda-Forno et al., 2023; Krishnamurthy et al., 2024; Monea et al., 2025; Schubert et al., 2024). Moreover, alignment and fine-tuning on human feedback and behavioral datasets can substantially increase human-likeness, in some cases matching the decision dynamics of traditional cognitive models (Bai et al., 2022; Ouyang et al., 2022; Binz et al., 2024; 2025; Momenté et al., 2025; Su et al., 2025). However, most evaluations in these settings emphasize the exploration–exploitation trade-off or overall performance, providing limited leverage for distinguishing between underlying strategies that could generate similar behavioral outcomes (Park et al., 2024a; Rahn et al., 2024; Nie et al., 2024; Felicioni et al., 2024). Our task departs from classical stochastic MABs by design: instead of conflating information gathering with reward maximization, it separates sampling from inference, which we find to be key to precisely assess alignment between LLMs and humans.

3. Active Probabilistic Reasoning Task

We introduce an *active probabilistic reasoning* task (Fig. 1A) inspired by classical decision-making and K -armed bandit paradigms (Lai and Robbins, 1985; Daw et al., 2006; Na-

jemnik and Geisler, 2005; Slivkins, 2019; Lattimore and Szepesvári, 2020), but explicitly designed to disentangle *sampling* from *inference*. The task is well-suited for modeling at the algorithmic level, and its structure is “simple” in comparison to many current benchmarks (Jimenez et al., 2023; Sprague et al., 2023; Liu et al., 2023b; Zhou et al., 2023; Mialon et al., 2023; Phan et al., 2025). This simplicity, however, is deceiving, as below we find that *CoT* reasoning is required for LLMs to achieve high performance in this task, and that even leading models still under-perform compared to humans in key aspects of the task.

Each trial is an independent game with a variable number of sampling rounds $N \in \{2, \dots, 15\}$ followed by a single inference round in which the agent must commit to a final decision. On each sampling round, the agent selects one of four buttons (A–D) and observes a binary outcome (RED/GREEN); at the start of game g , exactly one button is biased towards RED, emitting RED with probability $\alpha_B = 0.9$, while the remaining buttons are unbiased with $\alpha_U = 0.5$. The agent’s objective is to identify the biased button from the sampled evidence and report it in the inference round. Formally, the biased button is a latent variable $z_g \in \{1, \dots, 4\}$; at round t the agent chooses $a_t \in \{1, \dots, 4\}$ and observes $x_t \in \{0, 1\}$ (with $x = 1$ for RED). To promote active information acquisition, between 0 and 3 buttons are temporarily occluded on each round and thus unavailable.

Although this task resembles a K -armed bandit in its sequential action structure, it differs in computational goal and information structure: unlike standard bandits where choices yield rewards and agents maximize cumulative return via exploration–exploitation, here performance is determined solely by a one-shot final inference choice. Sampling choices carry no reward but only provide evidence about the single latent hypothesis (which button is biased). This separation enables independent assessment of sampling quality and inference quality.

4. Data Collection

We collect behavioral data from both human participants and language models. Human participants played an interactive, graphical version of the task¹. For language models, we designed an equivalent *text-based* version of the task, in which LLMs interact via token-defined choices under the same instructions provided to the human players (see Appendix B). Here we describe in detail the experimental procedures used for humans and language models.

Humans. We recruited 50 human participants for a 1-hour live in-person competition. All participants provided written informed consent prior to the task and received instructions matching those used to prompt the LLMs (Appendix B).

¹<https://ai.trt-bench.org>

Participants played multiple independent games with trial lengths sampled uniformly between 2 and 15 rounds. Of the 50 participants, 46 completed the full protocol of 100 games each, yielding 4,600 games in total (see Appendix E for individual participant performance profiles).

Large language models. We evaluate a broad set of models spanning the current LLM landscape, including both state-of-the-art closed-source systems and competitive open-weight models. The models range from *dense* to *Mixture-of-Experts* (MoE) architectures across different sizes and training paradigms: pre-trained, instruction fine-tuned, reasoning, and hybrid-reasoning models (Vaswani et al., 2017; Schulman et al., 2017; Shoeybi et al., 2019; Wei et al., 2021; Ouyang et al., 2022; Wei et al., 2022; Shu et al., 2023; Shao et al., 2024; Cai et al., 2025). Our model selection includes: OpenAI’s *gpt 4o mini* (Hurst et al., 2024), *gpt 4.1 mini* (OpenAI, 2025a), *gpt 5 mini* (OpenAI, 2025b), and the *gpt oss* open architectures in both the 20b and 120b parameter variants (OpenAI, 2025c); several *llama* models (Touvron et al., 2023; Dubey et al., 2024), including variants fine-tuned on human behavioral data (Binz et al., 2025); a distilled version of *deepseek* (Guo et al., 2025b); Anthropic’s *claude sonnet 4* and *claude haiku 3.5* (Anthropic, 2025); Google’s *gemini 2.5 pro/flash* and the smaller *gemma* models (Comanici et al., 2025; Gemma Team, Google DeepMind, 2025); the *qwen* family, including the 235B Mixture-of-Experts (MoE) model and earlier dense variants (Qwen Team, 2025; Yang et al., 2025); and the fully open-source *apertus* model (Hernández-Cano et al., 2025), *grok 3 mini* (xAI, 2025), and *glm 4.5* (Zeng et al., 2025). Some of the included reasoning models allow for control over *reasoning effort* (resulting in longer or shorter *chain-of-thoughts* token sequences); we evaluate their performance for both *low-* and *high-reasoning* effort. In all figures, results for the *high-reasoning* condition are shown with gray bars (see, e.g., Fig. 2A) and denoted as *Extended Reasoning*. For every LLM and reasoning condition, we evaluate a minimum of 1,400 individual games spanning uniformly the range of 2 to 15 rounds, amounting to more than 55,000 games in total.

5. Optimal Agent

To evaluate and compare the performance of LLMs and humans, we introduce an optimal agent that provides an upper bound on task performance. In our task, where inference and sampling are explicitly separated, establishing the optimal strategy for inference is straightforward: an agent should select the button with the highest posterior probability of being biased, following a *Maximum-A-Posteriori* (MAP) decision rule (Griffiths et al., 2008). This *optimal inference* strategy is defined as follows; button outcomes are generated by Bernoulli emissions, with the emission

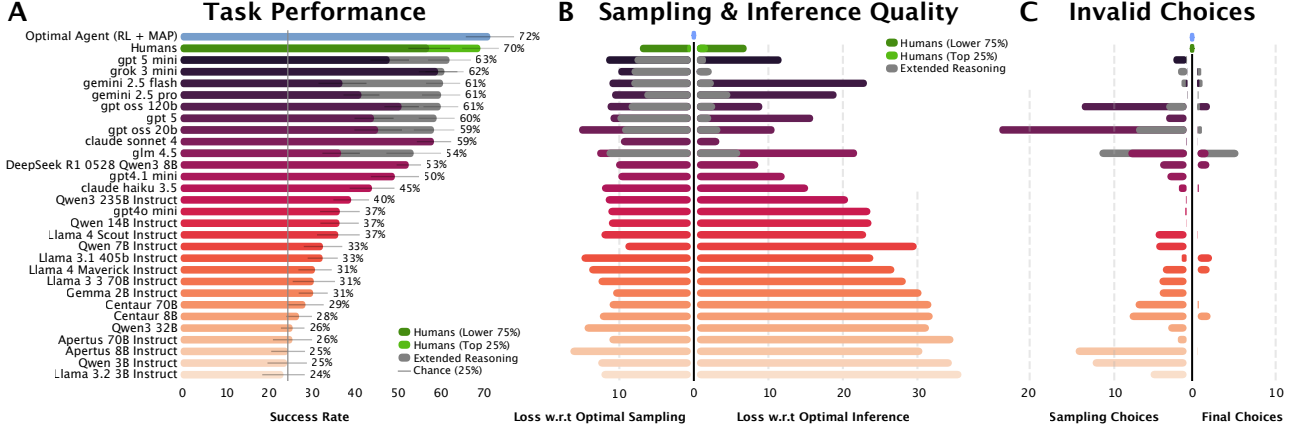


Figure 2. Comparing human and LLM behavior. **A: Task performance.** Average success rate across trial lengths $N \in \{2, \dots, 15\}$. We report human performance (green), split into lower 75% and top 25% of participants and the near-optimal reference agent (PPO sampling + MAP inference) (light blue). For models that support increased reasoning effort, gray overlays indicate the *Extended Reasoning* condition. Error bars represent standard deviations, computed across trial-cluster means with a uniform distribution over the number of rounds. The vertical line marks chance performance (25%). **B: Sampling and inference quality.** We quantify *sampling* quality (left) and *inference* quality (right) as performance loss with respect to the near-optimal agent (lower is better): inference loss is the gap between the agent and a counterfactual agent that preserves the same sampled evidence but applies MAP at the inference round for the final decision; sampling loss is the gap between this counterfactual MAP agent and the reference agent (PPO + MAP), isolating suboptimal evidence acquisition. Reasoning primarily reduces inference loss, with only modest effects on sampling loss. **C: Invalid choices.** Fraction of invalid choices during sampling (left) and at the final, *inference* decision (right). Invalid choices include selecting occluded options, producing tokens outside the valid choice set (A–D), or failing to respond; humans cannot produce invalid choices in the graphical interface. Invalid choices occur more frequently during sampling than at the final decision and are reduced by reasoning.

probabilities $\{\alpha_B, \alpha_U\}$ for the biased and unbiased buttons respectively. A single game g of N rounds consists of a sequence of choice-evidence pairs $(a_{1:N}, x_{1:N})$ together with a latent context variable $k \in \{1, \dots, K\}$. We represent beliefs by the posterior vector $(p_t)_k \in \Delta^K$. We also define the likelihoods over the latent variable k and emission rates $\{\alpha_B, \alpha_U\}$ by $(L_t)_k \in \Delta^K$. By assuming a uniform prior, we can write down the recursive normative posterior via Bayes' rule as²:

$$p_t = \frac{p_{t-1} \odot L_t}{\mathbf{1}^\top (p_{t-1} \odot L_t)}, \quad (p_0)_k = \frac{1}{4}. \quad (1)$$

where \odot denotes the Hadamard product. The MAP *inference* policy at round t selects the hypothesis with maximum posterior probability:

$$a_t^{\text{MAP}} := \arg \max_{k \in \{1, \dots, 4\}} (p_N)_k. \quad (2)$$

Determining the optimal *sampling* strategy is substantially more complex. The agent faces two sources of uncertainty: (1) buttons are randomly occluded at each round, restricting the available choice set at time t , $A_t \subseteq \{1, \dots, 4\}$ in unpredictable ways, and (2) the total number of sampling rounds $N \in \{2, \dots, 15\}$ is unknown to the agent until the inference round begins. These factors render analytical derivation of the optimal sampling policy non-trivial. Consequently, we employ reinforcement learning to obtain a

near-optimal sampling strategy. We train an RL agent using Proximal Policy Optimization (PPO) (Schulman et al., 2017); see Appendix C for full details. The resulting *optimal agent* combines the PPO-trained sampling policy with the MAP inference rule at the final decision round. We assume that this agent achieves near-ceiling performance and provides normative benchmarks for both *sampling* and *inference quality*.

6. Comparing Human & LLM Behavior

To compare human and LLM performance, we employ four complementary metrics that capture distinct aspects of behavior: (1) overall task performance, (2) sampling quality, (3) inference quality, and (4) invalid choice rates. Together, these metrics reveal a broad range of behaviors across LLMs, as well as systematic differences between LLM and human performance.

Overall task performance. In Figure 2A, we quantify *overall task performance* as the average *success rate* across all trial lengths ($N \in \{2, \dots, 15\}$), i.e., the fraction of games in which the agent correctly identifies the biased button at the inference round. Despite the task's simple structure, it induces a broad distribution of performance across both humans and models, and is sensitive to explicit reasoning, with clear gains from extended *chain-of-thought* (gray vs. colored bars). On average, human participants achieve $\simeq 61\%$ suc-

²See Appendix Section H.2.2 for derivation details.

cess, comparable to the best-performing LLM (*gpt 5 mini*); however, the top quartile of humans exceeds this level by $\sim 7\%$, highlighting wide human variability and a remaining gap between top models and skilled human players. Across models, reasoning LLMs outperform non-reasoning counterparts, attaining higher success rates overall. Success rates increase with game-length only for reasoning models; success rates in *low/no-reasoning* models remain largely flat, suggesting they largely fail to leverage the additional evidence provided by long games (Appendix D).

Sampling & inference quality. In Figure 2B, we quantify *inference quality* by computing the performance gap between each agent and a counterfactual agent that retains the same sampling strategy but applies the MAP inference rule at the final choice. This difference quantifies the performance loss attributable solely to suboptimal inference (right-hand side of Figure 2B, lower is better). We also evaluate *Sampling quality*, by comparing this counterfactual agent (which combines the agent’s sampling strategy with MAP inference) against the optimal agent defined above (which combines the RL-trained sampling policy with MAP inference). Since both agents share the optimal MAP inference rule, any remaining performance gap reflects the loss due to suboptimal sampling strategy (left-hand side of Fig. 2B, lower is better). We find that inference quality varies broadly across LLMs and is strongly correlated (negatively, because the metric is a loss) with overall performance ($r = -0.99$), whereas sampling quality is more homogeneous across LLMs and a weaker predictor of performance ($r = -0.47$; $r = -0.70$ if we include *extended reasoning* variants). Performance gains from extended reasoning are driven mainly by improved inference: for any given LLM, *chain-of-thought* reduces inference loss by an amount that largely mirrors the corresponding gain in overall performance. Notably, frontier reasoning models match, and sometimes exceed, humans in inference quality. In comparison, *extended reasoning* has only modest effects on sampling quality, and while the best reasoning models approach the performance of the lower 75% of human participants, skilled humans (top 25%) still substantially outperform LLMs in their sampling strategies (left-hand side of Fig. 2B; skilled humans shown in light green).

Invalid choice rates. Finally, in Figure 2C, we quantify *invalid choices* as the proportion of choices in which agents produce invalid responses during either sampling or inference. Invalid choices include selecting occluded buttons, generating output tokens outside the valid button vocabulary (A–D), or failing to produce a response altogether. By design, human participants cannot produce invalid choices in the graphical interface, and therefore invalid-choice rates are computed only for LLMs. Overall, we do not observe a statistically significant correlation between invalid choice rates and LLM performance; however, invalid choices are consis-

tently reduced under extended reasoning. Invalid responses tend to occur more often during sampling than during inference, potentially reflecting the changing availability of choices during the sampling rounds.

7. A mechanistic model of latent cognitive variables

The behavioral metrics above reveal systematic differences across LLMs, but do not identify the processes responsible for them. For instance, reasoning might improve inference by changing a single computation shared across models (e.g., evidence accumulation), by jointly affecting multiple computations within each model (e.g., evidence accumulation and internal biases), or by altering different computations in different models. To resolve these possibilities, we develop and fit a mechanistic model of *sampling* and *inference* for both humans and LLMs. The model draws on Bayesian ideal-observer and probabilistic cognition frameworks (Knill and Pouget, 2004; Sanborn et al., 2010) and parallels recent views of *in-context learning* as implicit inference over latent context variables (Xie et al., 2022; Panwar et al., 2024; Zhang et al., 2023), but allows for deviations from an ideal-observer in terms of memory accuracy, choice selection strategy and relative choice bias. The fitted parameters define four interpretable latent cognitive variables: **Memory**, **Strategy**, **Choice Bias**, and **Occlusion Awareness** placing agents in a *cognitive space* (Fig. 4A and schematically in Fig. 1D) spanned by the key parameters influencing decision strategy. This approach allows us to interpret key differences across LLMs and humans (Figs. 3, 4A).

Memory (β). As in traditional accounts of probabilistic inference in neuroscience and sequential sampling models (Busemeyer and Townsend, 1993; Usher and McClelland, 2001), we assume that an agent’s choices are a consequence of a non-optimal *memory* $h_t \in \mathbb{R}^K$ (Gold and Shadlen, 2007; Hogarth and Einhorn, 1992; Ma et al., 2023) and is updated via the mean subtracted likelihood:

$$\Delta h_t := \log L_t - \langle \log L_t \rangle \quad (3)$$

(See Appendix H.4.3 for details). After each sampling round, h_t is given by

$$h_t = (1 - \beta) h_{t-1} + \Delta h_t. \quad (4)$$

Deviations from optimal recollection of evidence are controlled by the memory parameter $\beta \in [-1, 1]$. For $\beta = 0$ accumulation of evidence is *perfect*; for $\beta > 0$ the agent is *forgetful*, leading to late evidence weighing more on choices than early one; and for $\beta < 0$ the agent is *stubborn*, leading to early evidence weighing more on choice than late one.

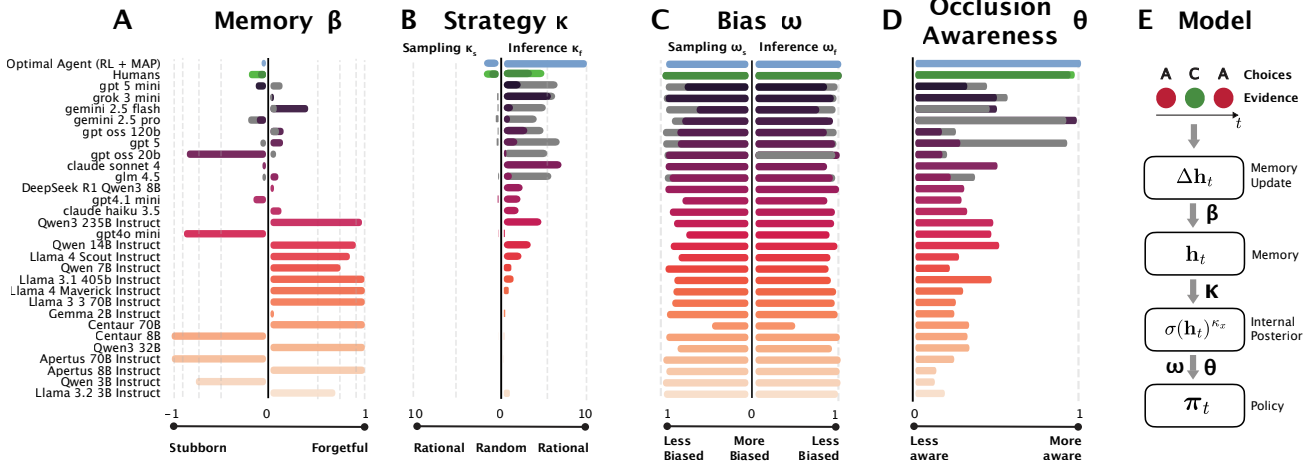


Figure 3. Model parameters explain human and LLM behavior **A:** Memory parameter β governs non-optimal evidence-integration, spanning *stubborn* ($\beta < 0$) to *forgetful* ($\beta > 0$) regimes. **B:** Strategy parameter κ controls choice stochasticity (*random* near $\kappa = 0$, increasingly *rational* for large κ), fit separately for sampling (left) and inference (right). **C:** Entropy of Choice-bias vector ω^x captures deviations from internal posterior-driven decisions, fit separately for sampling and inference (more biased for smaller entropy). **D:** Occlusion Awareness parameter (shown as $\log \theta$) captures sensitivity to occlusions (invalid choices). **E:** Model schematic: choices generate evidence that updates a Bayesian posterior p_t ; memory (β) produces a non-optimal information accumulation process h_t ; strategy (κ) applies an inverse-temperature transformation; bias (ω) and awareness (θ) modulate the resulting policy π_t .

Strategy (κ). After updating its memory state h_t based on new evidence, the agent converts h_t into an *internal posterior* $\bar{p}_t \in \Delta^K$ over which button is biased. We model this memory-to-belief transformation by multiplying h_t with a strategy parameter κ_x and re-normalizing, fit separately for *sampling* and *inference* ($x \in \{s, f\}$). This yields a continuum from near-random behavior ($\kappa_x \approx 0$) to increasingly *MAP-like* choices (large κ_x) (Ortega and Braun, 2013):

$$\bar{p}_t^x = \sigma(\kappa_x h_t), \quad (5)$$

For $\kappa_x > 1$, differences in accumulated evidence are amplified, producing sharper, more decisive behavior; for $\kappa_x < 1$ they are compressed, yielding a more diffuse posterior. In the limit $\kappa_x \gg 1$, the policy becomes effectively *MAP-like*, whereas $\kappa_x \approx 0$ yields near-uniform (*random*) choices. The *policy* for both *sampling* and *inference* choices is derived directly from \bar{p}_t^x .

Choice Bias (ω). To dissociate evidence-driven choices from systematic preferences, we include *choice biases* $\{\omega_s, \omega_f\} \in \Delta^K$ for the sampling and final choices, respectively (Gershman, 2020; Wei et al., 2024; Jiang et al., 2024). These normalized bias vectors act multiplicatively on the *internal posterior* to rescale the propensity for a choice independently of the sampled evidence. To quantify the strength of the bias in an agent, we compute the entropy of the bias vectors $H^x(\omega) = -\sum_j^x \omega_j^x \log(\omega_j^x)$. Unbiased agents distribute their choices uniformly in the absence of evidence, corresponding to large bias entropy. While, biased agents systematically favor one or more choices over others, corresponding to small bias entropy.

Occlusion Awareness (θ). To account for invalid sampling choices, we included the *occlusion awareness* parameter $\theta \in \mathbb{R}^{>0}$, which like the *choice biases* acts multiplicatively on the *internal posterior* (see ‘Policy’ below). We define a multiplicative mask $m_{t,j}^s$ as:

$$m_{t,j}^s = \theta^{-1\{\{j \notin \mathcal{A}_t\}}}, \quad (6)$$

where \mathcal{A}_t are the available choices at (t) . Large θ values result in an agent that is more occlusion-aware and avoids choosing occluded buttons while small θ values make the agent more prone to selecting occluded buttons.

Policy. Finally, the stochastic *policy* is obtained by combining the *internal posterior*, the *choices biases*, and *occlusion awareness*. We first define an un-normalized choice preference:

$$u_t^x := \bar{p}_t^x \odot \omega_x \odot m_t^x, \quad (7)$$

The preferences are then normalized to obtain the full *policy* $\pi_t^x = \frac{u_t^x}{1^T u_t^x}$ from which choices are sampled. The details of the model evaluation are described in Appendix E and full model derivations in Appendix H.

8. Reasoning aligns humans and LLMs

The parameters of the mechanistic model provide a compact description of the algorithms implemented by the agents we evaluated on the active probabilistic reasoning task (Fig. 3; parameter values are also shown in Appendix J). Critically,

this description is also accurate, as simulations of the mechanistic model based on the fitted parameters reproduce all main features of LLM and human behavior in our task (see Appendix F, Fig. 7).

We find that two model parameters are strongly related to overall LLM performance. First, the memory parameter β has values close to zero for all the highest performing models, indicating close to perfect accumulation of evidence. Poorly performing models instead tend to have large positive or negative β values, indicating either *forgetful* or *stubborn* accumulation of evidence (Fig. 3A). Second, the inference strategy parameter, κ_f , has larger values for better models (Fig. 3B). For the best models, we find $\kappa_f \gg 1$, implying a strategy that approximates a *maximum-a-posteriori* (MAP) policy. For models with intermediate performance, κ_f is closer to 1, meaning that information from the internal posterior is influencing final choices, but less so than expected from an optimal agent. Finally, for models with poor performance, κ_f progressively approaches zero, implying random choices and an inability to act on the observed evidence. Together, these trends in the memory and strategy parameters contribute to the improvements in inference quality observed in high-performing models (Fig. 2B).

However, other parameters also show substantial variation across LLMs, but weaker correlations with overall performance. Many poorly performing models, but also some high-performing ones, show substantial choice biases (Fig. 3C), which necessarily reduce sampling and/or inference quality. For any given LLM, the strength of sampling and inference biases is typically similar, suggesting a common underlying mechanism. LLMs also vary substantially in their occlusion awareness (Fig. 3D), resulting in widely different numbers of invalid choices across LLMs (Fig. 2C).

Across LLMs, *CoT* reasoning affects all four model parameters, albeit to different extents (Fig. 3A-D, gray vs. color bars). In most reasoning LLMs, a higher reasoning effort leads to β values closer to zero, indicating more accurate accumulation of evidence, and larger κ_f values, indicating a more rational *policy* on the final choice. Higher reasoning effort also reduces choice biases, during both sampling and inference, and increases occlusion awareness. Nonetheless, none of the tested LLMs can fully reproduce the algorithms employed by the optimal agent (Fig. 3A-D, blue bars). In particular, the inferred sampling strategy parameters κ_s are substantially smaller than those for the optimal agent or humans (Fig. 3B, left). This finding implies that sampling choices in LLMs are consistently less influenced by the observed evidence than the optimal agent, which explains the resulting gap in sampling quality discussed above (Fig. 2B, left).

Overall, *CoT* reasoning results in an increased alignment between the choice strategies used by LLMs and humans.

This increased alignment is best appreciated when mapping each agent onto a location in a *Cognitive Space* spanned by β and κ_f (Fig. 4A, and schematically in Fig. 1D). This summary representation shows how *CoT* pushes LLMs towards strategies that are closer to those used by skilled humans (Fig. 4A, light green dot) and that result in higher *overall performance* (Fig. 4A, background color and contours).

9. Reasoning shapes latent cognitive variables

Beyond summarizing the key features of the algorithms implemented by LLMs and humans, our mechanistic model also reveals latent cognitive variables whose dynamics reflect the operation of the distinct processes driving behavior (Fig. 3E). For example, our model implies that the final choice generated by an LLM reflects a *policy* that is obtained by accumulating all the sampled evidence into the *memory*, producing a strategy-sensitive *internal posterior*, and finally combining it with systematic biases.

These latent variables provide another view into the effects of *CoT* reasoning, as exemplified in Fig. 4B by the round-by-round dynamics of some of the inferred variables for a single game played by *gpt-oss-20b*, under *high-* (left) versus *low-*reasoning effort (right). We consider how the latent variables are updated on each round, during a game based on a specific sequence of RED and GREEN outcomes sampled across the four buttons (1st-row from top). Each outcome is transformed into a log-likelihood-ratio increment Δh_t (2nd-row) that can be accumulated into the optimal Bayesian posterior p_t (3rd-row). In our model, the Δh_t contribute to the *memory* state h_t (4th-row), which is then transformed into a *policy* for the final choice π_t (5th-row).

The dynamics of the resulting variables differ prominently across reasoning efforts. First, the *memory* state (h_t) is much more similar to the Bayesian posterior (p_t) for *high-* vs. *low-*reasoning effort. Midway through the example game, the Bayesian posterior switches from favoring *button C* to favoring *button A*, a dynamic reproduced by the *memory* state for *high-reasoning* (because $\beta \approx 0$). For *low-reasoning*, the *memory* state is *stubborn* ($\beta < 0$), and continues favoring the initially best option (*button C*) even in light of new evidence towards *A*. Second, reasoning affects the transformation of the *memory* into the *internal posterior*: *high-reasoning* sharpens this mapping, by favoring the best option on each round and ultimately resulting in a more *rational policy* ($\kappa_f \gg 1$). In contrast, *low-reasoning* weakens the differences between options in the *internal posterior*, which then results in a more diffuse *policy* (κ_f close to 0).

Such latent variables also amount to concrete, testable hypotheses for mechanistic interpretability, which aims to explain behavior at the implementation level by identifying

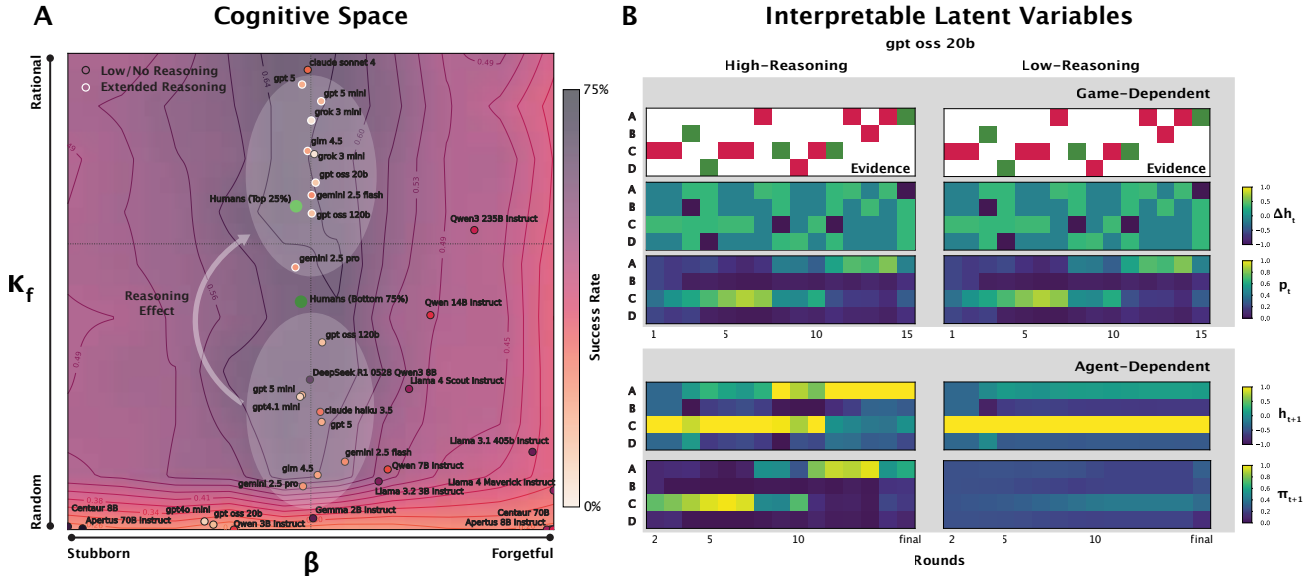


Figure 4. Reasoning aligns language models to human cognition. **A: Cognitive space.** Agents embedded by fitted *memory* β (stubborn $\beta < 0$ to *forgetful* $\beta > 0$) and *inference strategy* κ_f (more *rational* for larger κ_f). Near-optimal agent not shown (κ_f beyond y-axis limits). Shading/contours show predicted success across fitted model (β, κ_f); markers show humans (green/light green) and LLMs under low/no reasoning (black border) versus extended reasoning (white border). Reasoning shifts models toward the high-success, human-like regime. **B: Latent-variable dynamics.** Shows a specific evidence sequence (top row) and resulting round-by-round dynamics of latent variables (lower rows) during a game by *gpt oss 20b* under *high-* (left) vs. *low-*reasoning effort (right). *Game-dependent* terms (log-likelihood increments Δh_t and the posterior P_t) are identical across efforts, while *agent-dependent* quantities differ: *low-reasoning* yields a stubborn *memory state* trajectory h_t (4th row; $\beta < 0$) and diffuse *policy* π_t (5th row; smaller κ_f), whereas *high-reasoning* shows near-optimal *memory* updates ($\beta \approx 0$) and a sharper, more decisive belief-to-choice mapping (larger κ_f).

the circuits and causal pathways that give rise to it (Wang et al., 2022b; Hanna et al., 2023; Gurnee and Tegmark, 2023; Bereska and Gavves, 2024; Park et al., 2024b; Sharkey et al., 2025). Past efforts to understand *CoT* at the implementation level have yielded limited insights, in part because long reasoning traces expand the space of candidate computations and complicate causal attribution (Bogdan et al., 2025; Macar et al., 2025). Latent variables as in Fig. 4B (and Appendix Fig. 8B), have structure and dynamics that is much richer than the categorical (A–D) outputs required by the task, and as such motivate targeted questions about their representation: whether and where these latent variables are encoded in activations and circuits, which layers instantiate them, and how they evolve over the course of a *reasoning chain*.

10. Discussion

Our goal in this work was to understand whether language models form beliefs and make decisions under uncertainty in a human-like way, and how this alignment is affected by *chain-of-thought* (*CoT*) reasoning. We argued that answering these questions requires approaches that go beyond evaluating task performance alone, and instead rely on algorithmic descriptions that can isolate similarities and differences in the strategies implemented by different agents.

We applied this approach in a novel, *active probabilistic reasoning* task that disentangles *sampling* (active evidence acquisition) from *inference* (evidence integration) and employed a mechanistic model to infer interpretable, latent variables explaining each agent’s behavior.

Across LLMs, *CoT* reasoning is the key determinant of strong performance, but its effects are selective: reasoning leads to better performance primarily by improving *inference* rather than *sampling*. Mechanistically, improved inference is explained by (i) reduced choice biases (ω), (ii) a more *MAP-like* belief-to-choice mapping (larger inference strategy parameters κ_f) and, in strong models (iii) more accurate evidence-integration ($\beta \approx 0$). Together, these effects of reasoning move LLMs toward human-like regimes in *cognitive space* (Fig. 4B); sampling strategies, however, remain sub-optimal, leaving a persistent performance gap relative to skilled human sampling. Surprisingly, *CoT* reasoning in frontier LLMs leads to better alignment between humans and LLMs on our task than what is achieved by non-reasoning LLMs that were fine-tuned on human behavior from large corpora of cognitive tasks Binz et al. (2025).

Our work suggests a path toward LLM evaluations that measure capability while constraining underlying mechanisms, by asking not only *whether* models solve a task but *how* they do so. The resulting compact, algorithmic descriptions

of how reasoning changes LLM strategies provides concrete hypotheses for analyses at the implementation-level.

11. Reproducibility Statement

To ensure reproducibility of our results, all code used in our experiments, along with detailed instructions for setup and execution, is available at: https://drive.google.com/drive/folders/17tQx0021LN1VpwbOF_IIiM9oSm8DmRik.

Additionally, the active probabilistic reasoning task used for data collection is accessible at <https://ai.trt-bench.org>.

12. Impact Statement

This paper presents work whose goal is to advance our understanding of the field of Machine Learning through the lens of Cognitive Science. There are many potential societal consequences of our work, none which we feel must be specifically highlighted here.

References

Maxwell Nye, Anders Johan Andreassen, Guy Gur-Ari, Henryk Michalewski, Jacob Austin, David Bieber, David Dohan, Aitor Lewkowycz, Maarten Bosma, David Luan, et al. Show your work: Scratchpads for intermediate computation with language models. *arXiv:2112.00114*, 2021.

Laria Reynolds and Kyle McDonell. Prompt programming for large language models: Beyond the few-shot paradigm. In *Extended abstracts of the 2021 CHI conference on human factors in computing systems*, pages 1–7, 2021.

Jason Wei, Xuezhi Wang, Dale Schuurmans, Maarten Bosma, Fei Xia, Ed Chi, Quoc V Le, Denny Zhou, et al. Chain-of-thought prompting elicits reasoning in large language models. *Advances in neural information processing systems*, 35:24824–24837, 2022.

Takeshi Kojima, Shixiang Shane Gu, Machel Reid, Yutaka Matsuo, and Yusuke Iwasawa. Large language models are zero-shot reasoners. *Advances in neural information processing systems*, 35:22199–22213, 2022.

Xuezhi Wang, Jason Wei, Dale Schuurmans, Quoc Le, Ed Chi, Sharan Narang, Aakanksha Chowdhery, and Denny Zhou. Self-consistency improves chain of thought reasoning in language models. *arXiv preprint arXiv:2203.11171*, 2022a.

Qiguang Chen, Libo Qin, Jinhao Liu, Dengyun Peng, Jian-nan Guan, Peng Wang, Mengkang Hu, Yuhang Zhou, Te Gao, and Wanxiang Che. Towards reasoning era: A survey of long chain-of-thought for reasoning large language models. *arXiv preprint arXiv:2503.09567*, 2025a.

Aaron Jaech, Adam Kalai, Adam Lerer, Adam Richardson, Ahmed El-Kishky, Aiden Low, Alec Helyar, Aleksander Madry, Alex Beutel, Alex Carney, et al. Openai o1 system card. *arXiv preprint arXiv:2412.16720*, 2024.

Daya Guo, Dejian Yang, Haowei Zhang, Junxiao Song, Ruoyu Zhang, Runxin Xu, Qihao Zhu, Shirong Ma, Peiyi Wang, Xiao Bi, et al. Deepseek-r1: Incentivizing reasoning capability in llms via reinforcement learning. *arXiv preprint arXiv:2501.12948*, 2025a.

Ahmed El-Kishky, Alexander Wei, Andre Saraiva, Borys Minaiev, Daniel Selsam, David Dohan, Francis Song, Hunter Lightman, Ignasi Clavera, Jakub Pachocki, et al. Competitive programming with large reasoning models. *arXiv preprint arXiv:2502.06807*, 2025.

Miles Turpin, Julian Michael, Ethan Perez, and Samuel Bowman. Language models don’t always say what they think: Unfaithful explanations in chain-of-thought prompting. *Advances in Neural Information Processing Systems*, 36:74952–74965, 2023.

Tamera Lanham, Anna Chen, Ansh Radhakrishnan, Benoit Steiner, Carson Denison, Danny Hernandez, Dustin Li, Esin Durmus, Evan Hubinger, Jackson Kernion, et al. Measuring faithfulness in chain-of-thought reasoning. *arXiv preprint arXiv:2307.13702*, 2023.

Fazl Barez, Tung-Yu Wu, Iván Arcuschin, Michael Lan, Vincent Wang, Noah Siegel, Nicolas Collignon, Clement Neo, Isabelle Lee, Alasdair Paren, et al. Chain-of-thought is not explainability. *Preprint, alphaXiv*, page v1, 2025.

Yanda Chen, Joe Benton, Ansh Radhakrishnan, Jonathan Uesato, Carson Denison, John Schulman, Arushi Soman, Peter Hase, Misha Wagner, Fabien Roger, et al. Reasoning models don’t always say what they think. *arXiv preprint arXiv:2505.05410*, 2025b.

Iván Arcuschin, Jett Janiak, Robert Krzyzanowski, Senthooran Rajamanoharan, Neel Nanda, and Arthur Conmy. Chain-of-thought reasoning in the wild is not always faithful. *arXiv preprint arXiv:2503.08679*, 2025.

Arseny Moskvichev, Victor Vikram Odonard, and Melanie Mitchell. The conceptarc benchmark: Evaluating understanding and generalization in the arc domain. *arXiv preprint arXiv:2305.07141*, 2023.

David Marr. *Vision: A computational investigation into the human representation and processing of visual information*. MIT press, 2010.

Máté Lengyel. Marr's three levels of analysis are useful as a framework for neuroscience. *The Journal of Physiology*, 602(9):1911–1914, 2024. doi: 10.1113/JP279549. Epub 2024 Apr 16.

Alexander Ku, Declan Campbell, Xuechunzi Bai, Jiayi Geng, Ryan Liu, Raja Marjieh, R Thomas McCoy, Andrew Nam, Ilia Sucholutsky, Veniamin Veselovsky, et al. Using the tools of cognitive science to understand large language models at different levels of analysis. *arXiv preprint arXiv:2503.13401*, 2025.

Brenden M Lake, Tomer D Ullman, Joshua B Tenenbaum, and Samuel J Gershman. Building machines that learn and think like people. *Behavioral and brain sciences*, 40: e253, 2017.

Joshua C Peterson, David D Bourgin, Mayank Agrawal, Daniel Reichman, and Thomas L Griffiths. Using large-scale experiments and machine learning to discover theories of human decision-making. *Science*, 372(6547): 1209–1214, 2021.

Jason Wei, Maarten Bosma, Vincent Y Zhao, Kelvin Guu, Adams Wei Yu, Brian Lester, Nan Du, Andrew M Dai, and Quoc V Le. Finetuned language models are zero-shot learners. *arXiv preprint arXiv:2109.01652*, 2021.

Yuntao Bai, Andy Jones, Kamal Ndousse, Amanda Askell, Anna Chen, Nova DasSarma, Dawn Drain, Stanislav Fort, Deep Ganguli, Tom Henighan, et al. Training a helpful and harmless assistant with reinforcement learning from human feedback. *arXiv preprint arXiv:2204.05862*, 2022.

Long Ouyang, Jeffrey Wu, Xu Jiang, Diogo Almeida, Carroll Wainwright, Pamela Mishkin, Chong Zhang, Sandini Agarwal, Katarina Slama, Alex Ray, et al. Training language models to follow instructions with human feedback. *Advances in neural information processing systems*, 35:27730–27744, 2022.

Marcel Binz and Eric Schulz. Turning large language models into cognitive models. *arXiv preprint arXiv:2306.03917*, 2023a.

Filippo Momentè, Alessandro Suglia, Mario Giulianelli, Ambra Ferrari, Alexander Koller, Oliver Lemon, David Schlangen, Raquel Fernández, and Raffaella Bernardi. Triangulating LLM progress through benchmarks, games, and cognitive tests. In Christos Christodoulopoulos, Tanmoy Chakraborty, Carolyn Rose, and Violet Peng, editors, *Findings of the Association for Computational Linguistics: EMNLP 2025*, pages 20051–20072, Suzhou, China, November 2025. Association for Computational Linguistics. ISBN 979-8-89176-335-7. doi: 10.18653/v1/2025.findings-emnlp.1092. URL <https://aclanthology.org/2025.findings-emnlp.1092/>.

Marcel Binz, Elif Akata, Matthias Bethge, Franziska Brändle, Fred Callaway, Julian Coda-Forno, Peter Dayan, Can Demircan, Maria K. Eckstein, Noémi Éltető, Thomas L. Griffiths, Susanne Haridi, Akshay K. Jagadish, Li Ji-An, Alexander Kipnis, Sreejan Kumar, Tobias Ludwig, Marvin Mathony, Marcelo Mattar, Alireza Modirshanechi, Surabhi S. Nath, Joshua C. Peterson, Milena Rmus, Evan M. Russek, Tankred Saanum, Natalia Scharfenberg, Johannes A. Schubert, Luca M. Schulze Buschoff, Nishad Singh, Xin Sui, Mirko Thalmann, Fabian Theis, Vuong Truong, Vishaal Udandarao, Konstantinos Voudouris, Robert C. Wilson, Kristin Witte, Shuchen Wu, Dirk Wulff, Huadong Xiong, and Eric Schulz. A foundation model to predict and capture human cognition. *Nature*, 2025. doi: 10.1038/s41586-025-09215-4.

Tom Brown, Benjamin Mann, Nick Ryder, Melanie Subbiah, Jared D Kaplan, Prafulla Dhariwal, Arvind Neelakantan, Pranav Shyam, Girish Sastry, Amanda Askell, et al. Language models are few-shot learners. *Advances in neural information processing systems*, 33:1877–1901, 2020.

Shunyu Yao, Jeffrey Zhao, Dian Yu, Nan Du, Izhak Shaffran, Karthik R Narasimhan, and Yuan Cao. React: Synergizing reasoning and acting in language models. In *The eleventh international conference on learning representations*, 2022.

Michael Laskin, Luyu Wang, Junhyuk Oh, Emilio Parisotto, Stephen Spencer, Richie Steigerwald, DJ Strouse, Steven Hansen, Angelos Filos, Maxime Gazeau, et al. In-context reinforcement learning with algorithm distillation. *arXiv preprint arXiv:2210.14215*, 2022.

Noah Shinn, Federico Cassano, Ashwin Gopinath, Karthik Narasimhan, and Shunyu Yao. Reflexion: Language agents with verbal reinforcement learning. *Advances in Neural Information Processing Systems*, 36:8634–8652, 2023.

Zhihan Liu, Hao Hu, Shenao Zhang, Hongyi Guo, Shuqi Ke, Boyi Liu, and Zhaoran Wang. Reason for future, act for now: A principled framework for autonomous llm agents with provable sample efficiency. *arXiv preprint arXiv:2309.17382*, 2023a.

Xiao Liu, Hao Yu, Hanchen Zhang, Yifan Xu, Xuanyu Lei, Hanyu Lai, Yu Gu, Hangliang Ding, Kaiwen Men, Kejuan Yang, et al. Agentbench: Evaluating llms as agents. *arXiv preprint arXiv:2308.03688*, 2023b.

Qingxiu Dong, Lei Li, Damai Dai, Ce Zheng, Jingyuan Ma, Rui Li, Heming Xia, Jingjing Xu, Zhiyong Wu, Baobao Chang, et al. A survey on in-context learning. In *Proceedings of the 2024 conference on empirical methods in natural language processing*, pages 1107–1128, 2024.

Amir Moeini, Jiuqi Wang, Jacob Beck, Ethan Blaser, Shimon Whiteson, Rohan Chandra, and Shangtong Zhang. A survey of in-context reinforcement learning. *arXiv preprint arXiv:2502.07978*, 2025.

Martin Schrimpf, Idan Asher Blank, Greta Tuckute, Carina Kauf, Eghbal A Hosseini, Nancy Kanwisher, Joshua B Tenenbaum, and Evelina Fedorenko. The neural architecture of language: Integrative modeling converges on predictive processing. *Proceedings of the National Academy of Sciences*, 118(45):e2105646118, 2021.

Michael C Frank. Openly accessible llms can help us to understand human cognition. *Nature Human Behaviour*, 7(11):1825–1827, 2023.

Marcel Binz and Eric Schulz. Turning large language models into cognitive models. *arXiv preprint arXiv:2306.03917*, 2023b.

Gati V Aher, Rosa I Arriaga, and Adam Tauman Kalai. Using large language models to simulate multiple humans and replicate human subject studies. In *International conference on machine learning*, pages 337–371. PMLR, 2023.

Chenguang Zhao, Meirewuti Habule, and Wei Zhang. Large language models (llms) as research subjects: Status, opportunities and challenges. *New Ideas in Psychology*, 79: 101167, 2025.

Alyssa Loo, Ellie Pavlick, and Roman Feiman. Llms model how humans induce logically structured rules. *Journal of Memory and Language*, 146:104675, 2026.

Aleksandrs Slivkins. Introduction to multi-armed bandits. *Foundations and Trends® in Machine Learning*, 12(1-2): 1–286, 2019.

Tor Lattimore and Csaba Szepesvári. *Bandit algorithms*. Cambridge University Press, 2020.

Jonathan N Lee, Annie Xie, Chelsea Finn, Aldo Pacchiano, Yash Chandak, Ofir Nachum, and Emma Brunskill. Supervised pretraining can learn in-context reinforcement learning. In *Advances in Neural Information Processing Systems (NeurIPS)*, 2023.

Julian Coda-Forno, Marcel Binz, Zeynep Akata, Matthew Botvinick, Jane X Wang, and Eric Schulz. Meta-in-context learning in large language models. In *Advances in Neural Information Processing Systems (NeurIPS)*, 2023.

Akshay Krishnamurthy, Keegan Harris, Dylan J Foster, Cyril Zhang, and Aleksandrs Slivkins. Can large language models explore in-context? *Advances in Neural Information Processing Systems*, 37:120124–120158, 2024.

Giovanni Monea, Antoine Bosselut, Kianté Brantley, and Yoav Artzi. LLMs are in-context bandit reinforcement learners. In *Conference on Language Modeling (COLM)*, 2025.

Johannes A Schubert, Akshay K Jagadish, Marcel Binz, and Eric Schulz. In-context learning agents are asymmetric belief updaters. *arXiv preprint arXiv:2402.03969*, 2024.

Marcel Binz, Elif Akata, Matthias Bethge, Franziska Brändle, Fred Callaway, Julian Coda-Forno, Peter Dayan, Can Demircan, Maria K. Eckstein, Noémi Éltető, Thomas L. Griffiths, Susanne Haridi, Akshay K. Jagadish, Li Ji-An, Alexander Kipnis, Sreejan Kumar, Tobias Ludwig, Marvin Mathony, Marcelo Mattar, Alireza Modirshanechi, Surabhi S. Nath, Joshua C. Peterson, Milena Rmus, Evan M. Russek, Tankred Saanum, Natalia Scharfenberg, Johannes A. Schubert, Luca M. Schulze Buschoff, Nishad Singhi, Xin Sui, Mirko Thalmann, Fabian Theis, Vuong Truong, Vishaal Udandarao, Konstantinos Voudouris, Robert Wilson, Kristin Witte, Shuchen Wu, Dirk Wulff, Huadong Xiong, and Eric Schulz. Centaur: a foundation model of human cognition, 2024. URL <https://arxiv.org/abs/2410.20268>.

Ellen Su, Mark K. Ho, and Todd M. Gureckis. Integration of language and experience via the instructed bandit task. In *Proceedings of the 47th Annual Meeting of the Cognitive Science Society*, volume 47. Cognitive Science Society, 2025. URL <https://escholarship.org/uc/item/1j746305>. Conference paper.

Chanwoo Park, Xiangyu Liu, Asuman Ozdaglar, and Kaiqing Zhang. Do LLM agents have regret? a case study in online learning and games. *arXiv preprint arXiv:2403.16843*, 2024a.

Nate Rahn, Marc G Bellemare, and Pierluca D’Oro. Controlling large language model agents with entropic activation steering. *arXiv preprint arXiv:2406.00244*, 2024.

Allen Nie, Yi Su, Bo Chang, Jonathan N Lee, Ed H Chi, Quoc V Le, and Minmin Chen. EVOLVE: Evaluating and optimizing LLMs for exploration. *arXiv preprint arXiv:2410.06238*, 2024.

Nicolò Felicioni, Lucas Maystre, Sina Ghiassian, and Kamil Ciosek. On the importance of uncertainty in decision-making with large language models. *Transactions on Machine Learning Research*, 2024.

T. L. Lai and Herbert Robbins. Asymptotically efficient adaptive allocation rules. *Advances in Applied Mathematics*, 6(1):4–22, 1985. doi: 10.1016/0196-8858(85)90002-8.

Nathaniel D. Daw, John P. O'Doherty, Peter Dayan, Ben Seymour, and Raymond J. Dolan. Cortical substrates for exploratory decisions in humans. *Nature Neuroscience*, 9(6):867–873, 2006. doi: 10.1038/nn1743.

Jiri Najemnik and Wilson S. Geisler. Optimal eye movement strategies in visual search. *Nature*, 434:387–391, 2005. doi: 10.1038/nature03390.

Carlos E Jimenez, John Yang, Alexander Wettig, Shunyu Yao, Kexin Pei, Ofir Press, and Karthik Narasimhan. Swebench: Can language models resolve real-world github issues? *arXiv preprint arXiv:2310.06770*, 2023.

Zayne Sprague, Xi Ye, Kaj Bostrom, Swarat Chaudhuri, and Greg Durrett. Musr: Testing the limits of chain-of-thought with multistep soft reasoning. *arXiv preprint arXiv:2310.16049*, 2023.

Shuyan Zhou, Frank F Xu, Hao Zhu, Xuhui Zhou, Robert Lo, Abishek Sridhar, Xianyi Cheng, Tianyue Ou, Yonatan Bisk, Daniel Fried, et al. Webarena: A realistic web environment for building autonomous agents. *arXiv preprint arXiv:2307.13854*, 2023.

Grégoire Mialon, Clémentine Fourrier, Thomas Wolf, Yann LeCun, and Thomas Scialom. Gaia: a benchmark for general ai assistants. In *The Twelfth International Conference on Learning Representations*, 2023.

Long Phan, Alice Gatti, Ziwen Han, Nathaniel Li, Josephina Hu, Hugh Zhang, Chen Bo Calvin Zhang, Mohamed Shaaban, John Ling, Sean Shi, et al. Humanity's last exam. *arXiv preprint arXiv:2501.14249*, 2025.

Ashish Vaswani, Noam Shazeer, Niki Parmar, Jakob Uszkoreit, Llion Jones, Aidan N Gomez, Łukasz Kaiser, and Illia Polosukhin. Attention is all you need. *Advances in neural information processing systems*, 30, 2017.

John Schulman, Filip Wolski, Prafulla Dhariwal, Alec Radford, and Oleg Klimov. Proximal policy optimization algorithms. *arXiv preprint arXiv:1707.06347*, 2017.

Mohammad Shoeybi, Mostafa Patwary, Raul Puri, Patrick LeGresley, Jared Casper, and Bryan Catanzaro. Megatron-lm: Training multi-billion parameter language models using model parallelism. *arXiv preprint arXiv:1909.08053*, 2019.

Manli Shu, Jiong Xiao Wang, Chen Zhu, Jonas Geiping, Chaowei Xiao, and Tom Goldstein. On the exploitability of instruction tuning. *Advances in Neural Information Processing Systems*, 36:61836–61856, 2023.

Zhihong Shao, Peiyi Wang, Qihao Zhu, Runxin Xu, Junxiao Song, Xiao Bi, Haowei Zhang, Mingchuan Zhang, YK Li, Yang Wu, et al. Deepseekmath: Pushing the limits of mathematical reasoning in open language models. *arXiv preprint arXiv:2402.03300*, 2024.

Weilin Cai, Juyong Jiang, Fan Wang, Jing Tang, Sunghun Kim, and Jiayi Huang. A survey on mixture of experts in large language models. *IEEE Transactions on Knowledge and Data Engineering*, 2025.

Aaron Hurst, Adam Lerer, Adam P Goucher, Adam Perelman, Aditya Ramesh, Aidan Clark, AJ Ostrow, Akila Welihinda, Alan Hayes, Alec Radford, et al. Gpt-4o system card. *arXiv preprint arXiv:2410.21276*, 2024.

OpenAI. Gpt-4.1 mini — api model documentation, 2025a. Accessed 2025-09-23.

OpenAI. Gpt-5 system card. Technical report, OpenAI, 2025b. Accessed 2025-09-23.

OpenAI. gpt-oss-120b & gpt-oss-20b model card. *arXiv*, 2025c.

Hugo Touvron, Thibaut Lavril, Gautier Izacard, Xavier Martinet, Marie-Anne Lachaux, Timothée Lacroix, Baptiste Rozière, Naman Goyal, Eric Hambro, Faisal Azhar, et al. Llama: Open and efficient foundation language models. *arXiv preprint arXiv:2302.13971*, 2023.

Abhimanyu Dubey, Abhinav Jauhri, Abhinav Pandey, Abhishek Kadian, Ahmad Al-Dahle, Aiesha Letman, Akhil Mathur, Alan Schelten, Amy Yang, Angela Fan, et al. The llama 3 herd of models. *arXiv e-prints*, pages arXiv–2407, 2024.

Dong Guo et al. Deepseek-r1: Incentivizing reasoning capability in llms via reinforcement learning. *arXiv*, 2025b.

Anthropic. Claude opus 4 & claude sonnet 4 — system card. Technical report, Anthropic, 2025. Accessed 2025-09-23.

Gabriel Comanici et al. Gemini 2.5: Pushing the frontier with advanced reasoning, multimodality, long context, and next generation agentic capabilities. *arXiv*, 2025.

Gemma Team, Google DeepMind. Gemma 3 technical report. *arXiv*, 2025.

Qwen Team. Qwen3-235b (moe) — hugging face model card, 2025. Accessed 2025-09-23.

An Yang et al. Qwen3 technical report. *arXiv*, 2025.

Alejandro Hernández-Cano et al. Apertus: Democratizing open and compliant llms for global language environments. *arXiv*, 2025.

xAI. Grok 3 beta — the age of reasoning agents, 2025. Accessed 2025-09-23.

Aohan Zeng, Xin Lv, Qinkai Zheng, Zhenyu Hou, Bin Chen, Chengxing Xie, Cunxiang Wang, Da Yin, Hao Zeng, Jiajie Zhang, et al. Glm-4.5: Agentic, reasoning, and coding (arc) foundation models. *arXiv preprint arXiv:2508.06471*, 2025.

Thomas L. Griffiths, Charles Kemp, and Joshua B. Tenenbaum. Bayesian models of cognition. In Ron Sun, editor, *The Cambridge Handbook of Computational Psychology*, pages 59–100. Cambridge University Press, 2008. doi: 10.1017/CBO9780511816772.006.

David C. Knill and Alexandre Pouget. The Bayesian brain: the role of uncertainty in neural coding and computation. *Trends in Neurosciences*, 27(12):712–719, 2004. doi: 10.1016/j.tins.2004.10.007.

Adam N. Sanborn, Thomas L. Griffiths, and Daniel J. Navarro. Rational approximations to rational models: Alternative algorithms for category learning. *Psychological Review*, 117(4):1144–1167, 2010. doi: 10.1037/a0020511.

Sang Michael Xie, Aditi Raghunathan, Percy Liang, and Tengyu Ma. An explanation of in-context learning as implicit bayesian inference. In *International Conference on Learning Representations (ICLR)*, 2022. URL <https://openreview.net/forum?id=RdJVFCHjUMI>.

Madhur Panwar, Kabir Ahuja, and Navin Goyal. In-context learning through the Bayesian prism. In *International Conference on Learning Representations (ICLR)*, 2024. URL <https://openreview.net/forum?id=HX5ujdsSon>.

Yufeng Zhang, Fengzhuo Zhang, Zhuoran Yang, and Zhao-ran Wang. What and how does in-context learning learn? Bayesian model averaging, parameterization, and generalization. *arXiv preprint arXiv:2305.19420*, 2023. URL <https://arxiv.org/abs/2305.19420>.

Jerome R. Busemeyer and James T. Townsend. Decision field theory: A dynamic-cognitive approach to decision making in an uncertain environment. *Psychological Review*, 100(3):432–459, 1993. doi: 10.1037/0033-295X.100.3.432.

Marius Usher and James L. McClelland. The time course of perceptual choice: the leaky, competing accumulator model. *Psychological Review*, 108(3):550–592, 2001. doi: 10.1037/0033-295X.108.3.550.

Joshua I. Gold and Michael N. Shadlen. The neural basis of decision making. *Annual Review of Neuroscience*, 30: 535–574, 2007. doi: 10.1146/annurev.neuro.29.051605.113038.

Robin M. Hogarth and Hillel J. Einhorn. Order effects in belief updating: The belief-adjustment model. *Cognitive Psychology*, 24(1):1–55, 1992. doi: 10.1016/0010-0285(92)90002-J.

Wei Ji Ma, Konrad Paul Kording, and Daniel Goldreich. *Bayesian Models of Perception and Action: An Introduction*. The MIT Press, Cambridge, MA, 2023. ISBN 9780262047593. Hardcover. eBook ISBN: 9780262372824.

Pedro A. Ortega and Daniel A. Braun. Thermodynamics as a theory of decision-making with information-processing costs. *Proceedings of the Royal Society A: Mathematical, Physical and Engineering Sciences*, 469(2153):20120683, May 2013. doi: 10.1098/rspa.2012.0683.

Samuel J. Gershman. Origin of perseveration in the trade-off between reward and complexity. *Cognition*, 204:104394, November 2020. doi: 10.1016/j.cognition.2020.104394.

Sheng-Lun Wei, Cheng-Kuang Wu, Hen-Hsen Huang, and Hsin-Hsi Chen. Unveiling selection biases: Exploring order and token sensitivity in large language models. In Lun-Wei Ku, Andre Martins, and Vivek Srikumar, editors, *Findings of the Association for Computational Linguistics: ACL 2024*, pages 5598–5621, Bangkok, Thailand, August 2024. Association for Computational Linguistics. doi: 10.18653/v1/2024.findings-acl.333.

Bowen Jiang, Yangxinyu Xie, Zuoqun Hao, Xiaomeng Wang, Tanwi Mallick, Weijie J Su, Camillo Jose Taylor, and Dan Roth. A peek into token bias: Large language models are not yet genuine reasoners. In Yaser Al-Onaizan, Mohit Bansal, and Yun-Nung Chen, editors, *Proceedings of the 2024 Conference on Empirical Methods in Natural Language Processing*, pages 4722–4756, Miami, Florida, USA, November 2024. Association for Computational Linguistics. doi: 10.18653/v1/2024.emnlp-main.272.

Kevin Wang, Alexandre Variengien, Arthur Conmy, Buck Shlegeris, and Jacob Steinhardt. Interpretability in the wild: a circuit for indirect object identification in gpt-2 small. *arXiv preprint arXiv:2211.00593*, 2022b.

Michael Hanna, Ollie Liu, and Alexandre Variengien. How does gpt-2 compute greater-than?: Interpreting mathematical abilities in a pre-trained language model. *Advances in Neural Information Processing Systems*, 36:76033–76060, 2023.

Wes Gurnee and Max Tegmark. Language models represent space and time. *arXiv preprint arXiv:2310.02207*, 2023.

Leonard Bereska and Efstratios Gavves. Mechanistic interpretability for ai safety—a review. *arXiv preprint arXiv:2404.14082*, 2024.

Core Francisco Park, Andrew Lee, Ekdeep Singh Lubana, Yongyi Yang, Maya Okawa, Kento Nishi, Martin Wattenberg, and Hidenori Tanaka. Iclr: In-context learning of representations. *arXiv preprint arXiv:2501.00070*, 2024b.

Lee Sharkey, Bilal Chughtai, Joshua Batson, Jack Lindsey, Jeff Wu, Lucius Bushnaq, Nicholas Goldowsky-Dill, Stefan Heimersheim, Alejandro Ortega, Joseph Bloom, et al. Open problems in mechanistic interpretability. *arXiv preprint arXiv:2501.16496*, 2025.

Paul C Bogdan, Uzay Macar, Neel Nanda, and Arthur Conmy. Thought anchors: Which llm reasoning steps matter? *arXiv preprint arXiv:2506.19143*, 2025.

Uzay Macar, Paul C Bogdan, Senthooran Rajamanoharan, and Neel Nanda. Thought branches: Interpreting llm reasoning requires resampling. *arXiv preprint arXiv:2510.27484*, 2025.

Nathaniel D. Daw. Trial-by-trial data analysis using computational models: (tutorial review). In Mauricio R. Delgado, Elizabeth A. Phelps, and Trevor W. Robbins, editors, *Decision Making, Affect, and Learning: Attention and Performance XXIII*. Oxford University Press, 2011. doi: 10.1093/acprof:oso/9780199600434.003.0001. URL <https://doi.org/10.1093/acprof:oso/9780199600434.003.0001>.

Christopher M. Bishop. *Pattern Recognition and Machine Learning*. Springer, New York, 2006.

Contents

A Limitations and Future Work	16
B Prompting Structure used for the LLMs in the Task	17
C Reinforcement Learning Agent Details	18
D Task Performance across Rounds	19
E Human Participants	20
F Mechanistic Model reproduces Behavioral Metrics	21
G Latent variable dynamics: Stubborn and Forgetful Examples	22
H Model Formulation Details	23
H.1 Introduction	23
H.1.1 Active Probabilistic Reasoning Task	23
H.2 Normative Bayes Posterior	23
H.2.1 Bayes posterior in scalar form	24
H.2.2 Stepwise Bayes update	24
H.2.3 Bayes update in probability space	25
H.2.4 Log-integrator equation	25
H.3 Log-ratio accumulator	26
H.3.1 Log-ratio evidence	26
H.3.2 δ_t evidence recursive equation	27
H.3.3 Recovering the original log-integrator	27
H.4 Memory Bayesian Integrator	28
H.4.1 Equivalence with the accumulator q_t	28
H.4.2 Evidence increments in centered log space	29
H.4.3 Memory state update	30
H.5 Internal posterior and Policy	30
H.5.1 Internal posterior	30
H.5.2 Occlusion mask	30
H.6 Model loss function	31
I Fitting Results	32
J Model Fitting Parameters	38

A. Limitations and Future Work

Our task and mechanistic model provide a step toward evaluations that move beyond final accuracy, which here allowed us to disentangle *sampling* from *inference* and to map both humans and LLMs into a shared space of interpretable latent variables. This framing yields a compact, process-level account of behavior and makes concrete, testable predictions. At the same time, some modeling and benchmarking choices trade expressivity for interpretability, suggesting clear directions for improvement.

(1) Coarse belief dynamics via a single leak parameter β . We summarize memory with a single leak parameter β , which imposes one global timescale for evidence retention across all rounds and both task phases (sampling vs. final choices). This constraint improves interpretability and comparability, but cannot capture richer dynamics such as nonstationary integration of evidence, context-dependent leakage across rounds, or within-game regime switches. Future work could extend the model to include different internal memory h_t integrators for *sampling* and *inference*, testing whether the observed *stubborn* and *forgetful* regimes reflect a single computation or a mixture of mechanisms that *CoT* modulates selectively.

(2) Round-invariant parameters, especially the sampling strategy κ_s . Several parameters are assumed constant within a game, most notably the sampling strategy κ_s . Empirically, posterior trajectories for inference are well captured by the fitted model, whereas sampling posteriors in very specific cases are less accurately predicted, with deviations suggestive of within-game adaptation. The sampling curves shown in Appendix Figs. 9–12 show sampling posterior trajectories with different curvature dynamics than the ones observed in the *inference* posteriors (note in particular the trajectories for the top models). One plausible interpretation is *in-context learning*: as evidence accumulates, the belief-to-sampling mapping becomes sharper. Allowing a round-dependent $\kappa_s(t)$ (or a simple update rule for κ_s) would directly test this hypothesis and may improve the sampling posterior fits. This can be intuitively understood as the model changing its propensity for *MAP-like* sampling as it gathers evidence. Importantly, even though posterior trajectories are in some cases imperfectly fit, they provide additional, direct support for our main conclusions: sampling and inference dissociate, and extended reasoning primarily improves inference while leaving a systematic gap in active information acquisition. Our hypothesis is that the task mode switching that happens when transitioning from *sampling* to *inference* leads to a different computation to be performed on the evidence, as in the *inference* round all the evidence has been accumulated and so a more clear decision can be made, leading to higher κ 's. In contrast, in settings when more exploration is needed, like early in sampling, lower κ 's dominate.

(3) No closed-form optimal sampler under occlusions and unknown horizon. Our benchmark relies on a near-optimal PPO policy as a reference sampler because the analytically optimal sampling policy is non-trivial under stochastic occlusions and an unknown number of rounds. Stronger optimality guarantees would further sharpen the decomposition into sampling versus inference losses.

(4) A single set of task meta-parameters. Because collecting statistically reliable human data and running large-scale evaluations across a broad set of LLMs is expensive and time-consuming, we focus on a single regime of task meta-parameters (number of buttons, emission probabilities, occlusion process, and horizon distribution). Different regimes may induce qualitatively different optimal strategies and could change both the magnitude and the nature of *CoT* effects, motivating systematic sweeps over these task parameters.

(5) Reasoning traces are not analyzed. We focus on behavior and latent-variable fits, but do not analyze the *reasoning traces* themselves. Combining trace-level analyses with latent variables could test *whether* (and *when*) explicit *CoT* content tracks inferred belief states versus serving as a post-hoc narrative, and could identify trace features predictive of latent parameters (e.g., signatures of evidence accumulation or policy sharpening). More broadly, this would open a natural path for future mechanistic interpretability work: using trace-linked latent variables as targeted probes to ask *where* (and *how*) quantities like p_t , h_t , or κ -like belief-to-policy transformations are instantiated in model activations and circuits.

Overall, our framework points toward a next generation of evaluations: benchmarks that measure capability while constraining the computations that produce it, and mechanistic models that translate behavior into algorithmic variables, setting the stage for implementation-level tests of how reasoning is realized in language-model circuits.

B. Prompting Structure used for the LLMs in the Task

We evaluate language models using a text-based version of the task that mirrors the instructions and feedback given to human participants. The prompt specifies the task mechanics (four cues, one biased at 90/10 while the others are 50/50), the round-by-round interaction protocol (available cues may change across rounds, but at least one cue is always available), and a strict response format (one letter per round, no additional text). After the sampling rounds, models are asked to report which cue had the highest proportion of RED outcomes. The prompt also defines the feedback and scoring scheme (correct/incorrect/invalid; +100 for a correct final report and -100 otherwise), explicitly framing success as identifying the biased cue. Models interact with the environment across full trials and receive round- and trial-specific updates conditional on their previous choices.

Active Probabilistic Reasoning Task Prompt

Task

- You will play a game with $\{n_rounds\}$ rounds.
- In each round, some cues are available: A, B, C, D.
- One cue is biased: 90% one color / 10% the other. The others are 50/50.
- Available cues may disappear at random, but at least one is always active.
- Each round, respond with exactly one letter (A, B, C, or D). No markup or punctuation.
- After $\{n_rounds\}$ rounds, identify the biased cue.
- Scoring: Correct +100 points, Wrong -100 points.

Round prompt

- ``Trial X, Round $\{current_round\}$: Available cues $\{available_cues\}$. Which do you choose? Respond with exactly one letter: A, B, C, or D.''

Round feedback

- ``Trial X, Round $\{current_round\}$: Available cues $\{available_cues\}$. You chose ``CURRENT_ANSWER'' and saw ``RESULT''.''

Final decision prompt

- ``Trial X: Based on all observed colors, which cue $\{letters\}$ had the highest ratio of RED? Respond with exactly one letter: A, B, C, or D.''

Final feedback

- ``Trial X: Based on all observed colors, which cue $\{letters\}$ had the highest ratio of RED?
You chose ``CURRENT_ANSWER'' which was ``FEEDBACK-CORRECT/INCORRECT''.
You received $\{score\}$ points.''

Feedback labels

- Correct: ``the biased cue''
- Incorrect: ``not the biased cue. The biased cue was ``BIASED_QUADRANT''.''
- Invalid: ``an invalid choice''

C. Reinforcement Learning Agent Details

We train a reinforcement-learning agent to obtain a near-optimal sampling policy for our task. Training is performed with Proximal Policy Optimization (PPO) (Schulman et al., 2017). At each round, the agent observes a 12-dimensional state vector consisting of (i) cue–color counts for each button (8 dimensions: 4 cues \times 2 colors) and (ii) a 4-dimensional binary mask indicating which cues are currently available. Environment dynamics (cue bias, occlusions, and trial length) match the experimental task, with the number of rounds N sampled uniformly from $\{2, \dots, 15\}$.

During the sampling phase, the PPO policy selects which cue to sample. At the end of the trial, the agent makes a final decision using a Maximum-A-Posteriori (MAP) rule given the accumulated evidence. Rewards are sparse and tied to task success: the agent receives +100 for a correct final report, 0 for valid sampling choices, and -10 for selecting an unavailable cue. Unavailable selections advance the round without revealing evidence, encouraging the agent to avoid invalid choices and sample efficiently.

We select optimization and architecture hyperparameters via a grid search that maximizes correct cue identification. The policy network is a two-layer MLP with 64 hidden units per layer and ReLU activations. We train for 5×10^6 environment steps with learning rate 2×10^{-5} and minibatch size 128. Each PPO iteration collects $T = 2048$ on-policy steps and performs 10 optimization epochs. We use discount $\gamma = 0.99$, generalized advantage estimation $\lambda_{\text{GAE}} = 0.95$, and clipping parameter $\varepsilon = 0.2$, with entropy and value loss coefficients set to 0.01 and 0.5, respectively.

D. Task Performance across Rounds

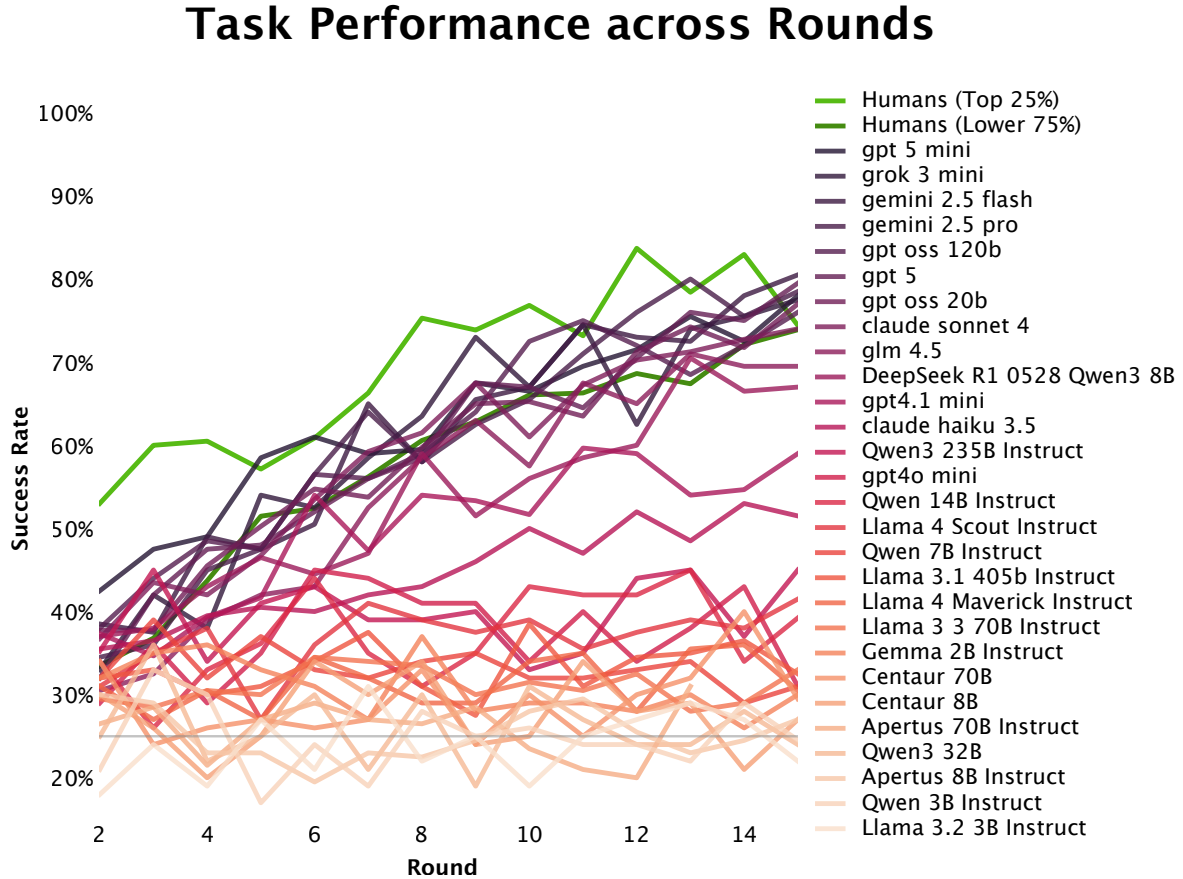


Figure 5. Evolution of success rate across rounds. For each agent, we report the mean success rate (fraction of trials in which the final reported button is the true biased one) as a function of the number of sampling rounds $N \in \{2, \dots, 15\}$. Humans are shown in green, split into the top 25% and lower 75% of participants (same split as in Fig. 2A); LLMs are shown as individual traces (legend), with colors indicating each model’s overall average success rate (lighter/orange = lower, darker/purple = higher). Across models, this view reveals a qualitative separation around $\sim 45\%$ average success: below this regime, curves remain approximately flat with increasing N , suggesting limited ability to convert additional evidence into improved final decisions; above it, curves exhibit a clear positive slope (“lift-off”), indicating effective inference in longer games. *Claude haiku 3.5* is the first model in the performance ranking to show this lift-off, and from *DeepSeek R1 0528 Qwen3 8B* onward, many models track the round-by-round improvement profile of the lower 75% human cohort. Overall, models that display lift-off are predominantly those with extended reasoning.

E. Human Participants

We collected human data in a 1-hour, live in-person session. Fifty participants took part and provided written informed consent. Participants played independent games of our task with trial length sampled uniformly from $N \in \{2, \dots, 15\}$ under the same instructions used throughout the paper (Fig. 1A). Forty-six participants completed the full protocol of 100 games each; all analyses in the main text therefore use these $46 \times 100 = 4,600$ trials.

Figure 6 reports participant-level performance and decomposes it into inference versus sampling components, complementing the aggregate human summary in Fig. 2. Human success rates span a wide range (roughly 37%–77%; chance = 25%), with most participants clustered around $\sim 55\%-67\%$. This heterogeneity is informative for our central comparison: the human distribution overlaps the best LLMs in overall success, while the strongest participants remain a meaningful reference point for what robust inference *and* effective sampling look like in this task.

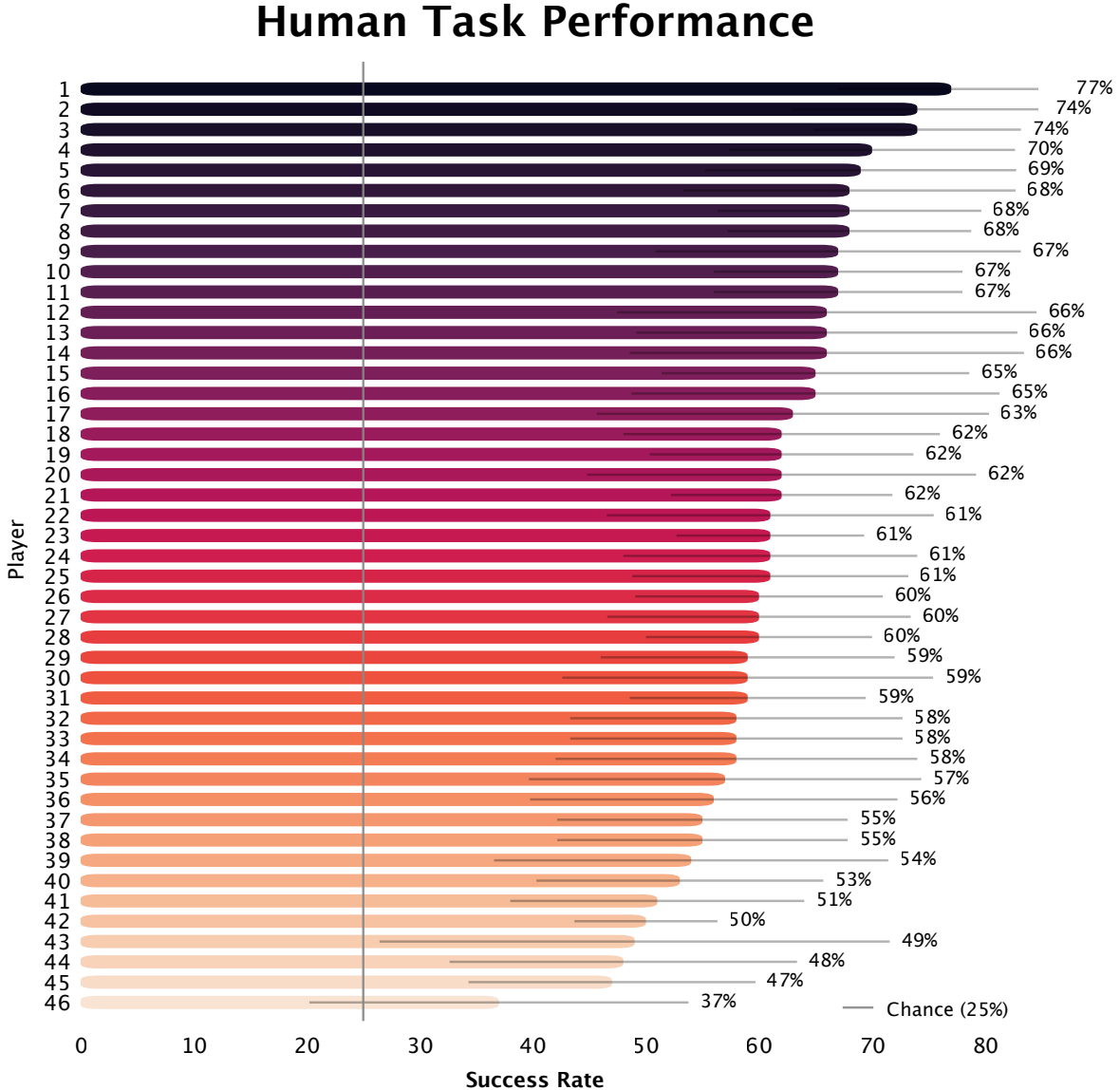


Figure 6. Individual human performance. Each row corresponds to one of the 46 participants who completed 100 games (trial lengths uniformly sampled from $N \in \{2, \dots, 15\}$). Participants are ordered by mean success rate. Mean success rate (correct identification of the biased option at the final decision); the vertical line marks chance performance (25%). The cohort exhibits substantial heterogeneity, spanning $\approx 37\%$ to $\approx 77\%$ success, with most participants concentrated around $\sim 55\%-67\%$.

F. Mechanistic Model reproduces Behavioral Metrics

Model evaluation is performed by simulating the fitted model policy on the *Active Probabilistic Reasoning Task*. For each model and reasoning condition parameters, we roll out full games with the same underlying $\{\alpha_B, \alpha_U\}$ parameters as in the Human and LLM experiment. At each round, the internal memory representation is updated from the initial posterior and a sampling policy is formed from the *choice bias* and *internal posterior*. The comparative posterior/bias plots can be seen in Fig. 7 and represents the average evolution of the underlying posteriors across games with $\{2, \dots, 15\}$ rounds, split by sampling and inference components.

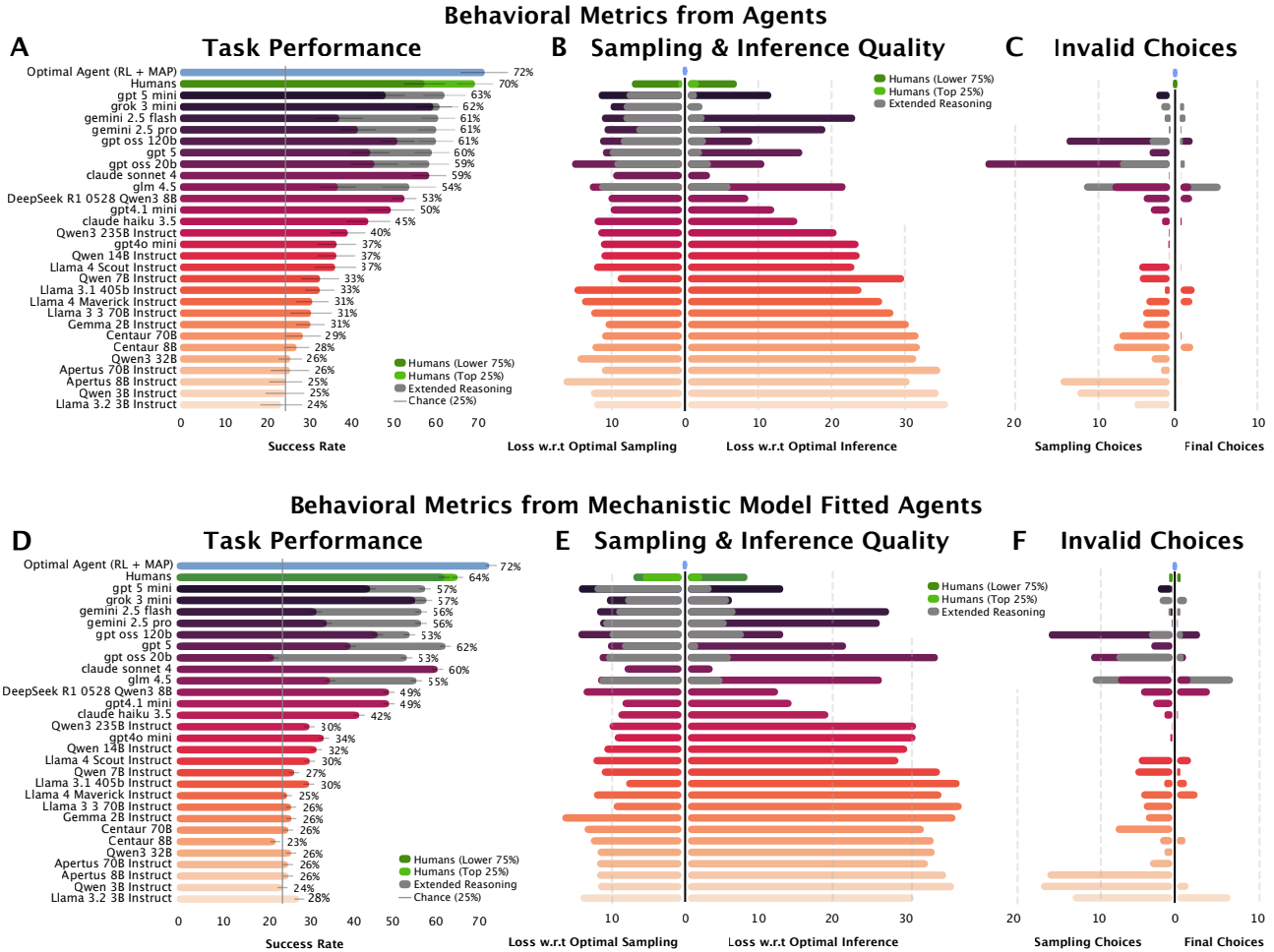


Figure 7. Behavioral metrics are recapitulated by the fitted mechanistic model. **A–C:** Empirical behavioral metrics computed directly from human and LLM trajectories. **A:** Overall task performance (success rate) across agents. **B:** Decomposition of performance loss into *sampling* versus *inference* deficits, measured by comparing each agent to counterfactual and optimal reference policies (loss w.r.t. optimal sampling on the left; loss w.r.t. optimal inference on the right). **C:** Invalid-choice rates during sampling and final report. **D–F:** The same metrics computed from trajectories generated by the *mechanistic model* after fitting $(\beta, \kappa, \omega, \theta)$ to each agent. **D:** Model-predicted success rates closely match empirical performance ordering. **E:** Model reproduces the sampling–inference loss decomposition, capturing that reasoning primarily reduces inference loss while leaving a residual sampling gap. **F:** Model reproduces invalid-choice profiles via the occlusion-awareness component. Green markers denote human quartiles; grey indicates extended-reasoning conditions.

G. Latent variable dynamics: Stubborn and Forgetful Examples

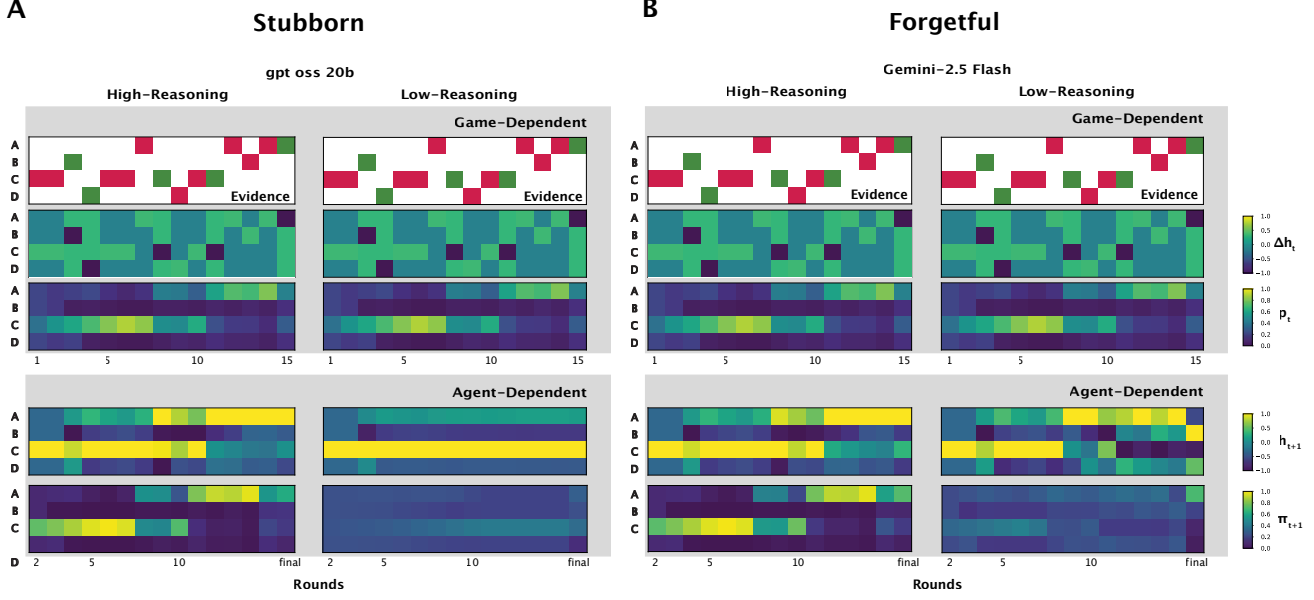


Figure 8. Stubborn vs. forgetful latent dynamics under reasoning. For both models we show how the latent variables are updated on each round, during a game based on a specific sequence of red and green outcomes sampled across the four buttons under *high*-reasoning (left) and *low*-reasoning (right). The top block (*game-dependent*) shows the sampled evidence sequence and the corresponding log-likelihood increments Δh_t and normative posterior p_t (computed from Eq. 1), which are identical across reasoning conditions for the same game. The bottom block (*agent-dependent*) shows the fitted internal belief state h_t and the induced policy π_t (rows: buttons A–D; columns: rounds and final decision). **A: Stubborn (gpt oss 20b).** Under *low*-reasoning, gpt oss 20b exhibits a stubborn regime ($\beta < 0$), with h_t dominated by early evidence and a comparatively diffuse belief-to-choice mapping; higher reasoning shifts h_t toward cleaner integration ($\beta \approx 0$) and sharpens π_t (larger κ_f). **B: Forgetful (Gemini-2.5 Flash).** In contrast, Gemini-2.5 Flash is forgetful under low reasoning ($\beta > 0$), over-weighting recent evidence; extended reasoning reduces leakage and sharpens the final policy, yielding more stable integration and more MAP-like choices.

H. Model Formulation Details

H.1. Introduction

We define this model under a set of cognitive assumptions: agents can be biased, forgetful or stubborn, can ignore the occlusions thus making invalid choices and can exploit in a MAP-like way or explore randomly. The goal is to parameterize these departures from an ideal observer, so that each fitted agent can be characterized in terms of (i) how evidence is integrated over time, and (ii) how beliefs are translated into choices.

We start by defining the normative Bayesian model and the quantities needed to build a stepwise belief integrator from observations generated by the **Active Probabilistic Reasoning Task**. This provides a reference point (the ideal observer) against which non-optimal integration and biased choice rules can be measured against.

H.1.1. ACTIVE PROBABILISTIC REASONING TASK

We consider independent games of each with $t \in \{1, \dots, N\}$ rounds consisting of t sampling rounds followed by one final choice where K choices are potentially available; in our version of the task, $K = 4$.

Latent target and observations. Each game has a latent target $z \in \{1, \dots, K\}$ with prior

$$\Pr(z = k) = p_0(k), \quad p_0(k) > 0. \quad (8)$$

At sampling round $t \in \{1, \dots, N\}$, the agent chooses an arm $a_{g,t} \in \{1, \dots, K\}$ and observes a binary outcome $x_t \in \{0, 1\}$ (e.g. $x = 1$ = RED, $x = 0$ = GREEN).

Shared-rate Bernoulli emission model. We assume a shared-rate Bernoulli model with parameters $0 < \alpha_U < \alpha_B < 1$. Defining the Bernoulli pmf $\text{Ber}(x; \theta) := \theta^x(1 - \theta)^{1-x}$, the emission model is

$$\Pr(x_t = 1 \mid a_t = i, z = k) = \begin{cases} \alpha_B & \text{if } k = i, \\ \alpha_U & \text{if } k \neq i, \end{cases} \quad (9)$$

$$\Pr(x_t = 0 \mid a_t = i, z = k) = 1 - \Pr(x_t = 1 \mid a_t = i, z = k). \quad (10)$$

Equivalently,

$$\Pr(x_t \mid a_t = i, z = k) = \begin{cases} \text{Ber}(x_t; \alpha_B) & k = i, \\ \text{Ber}(x_t; \alpha_U) & k \neq i. \end{cases} \quad (11)$$

Conditional independence across rounds. Given z and the choices, outcomes are conditionally independent across rounds:

$$p(x_{1:N} \mid a_{1:N}, z_n = k) = \prod_{t=1}^N p(x_t \mid a_t, z = k). \quad (12)$$

H.2. Normative Bayes Posterior

Let the latent context be $z \in \{1, \dots, K\}$ with prior

$$\mathbf{p}_0 \in \Delta^K, \quad (\mathbf{p}_0)_k = \Pr(z = k). \quad (13)$$

On each game g , the agent makes a sequence of choices $a_{1:t}$ and observes evidence $x_{1:t}$, so if we assume conditional independence across trials given z :

$$p(x_{1:t} \mid a_{1:t}, z = k) = \prod_{r=1}^t p(x_r \mid a_r, z = k). \quad (14)$$

Equation (14) is the (factorized) likelihood of the data up to round t and evidence sequence $x_{1:t}$ under hypothesis $z = k$, conditional on the choices $a_{1:t}$.

H.2.1. BAYES POSTERIOR IN SCALAR FORM

For a single hypothesis $k \in \{1, \dots, K\}$, define the scalar posterior

$$p_t(k) := \Pr(z = k \mid a_{1:t}, x_{1:t}). \quad (15)$$

Applying Bayes' rule and using the factorization (14),

$$\begin{aligned} p_t(k) &= \frac{\Pr(z = k) p(x_{1:t} \mid a_{1:t}, z = k)}{\sum_{j=1}^K \Pr(z = j) p(x_{1:t} \mid a_{1:t}, z = j)} \\ &= \frac{(\mathbf{p}_0)_k \prod_{r=1}^t p(x_r \mid a_r, z = k)}{\sum_{j=1}^K (\mathbf{p}_0)_j \prod_{r=1}^t p(x_r \mid a_r, z = j)}. \end{aligned} \quad (16)$$

Defining the per-round likelihood

$$L_r(k) := p(x_r \mid a_r, z = k), \quad (17)$$

equation (16) can be written compactly as

$$p_t(k) = \frac{(\mathbf{p}_0)_k \prod_{r=1}^t L_r(k)}{\sum_{j=1}^K (\mathbf{p}_0)_j \prod_{r=1}^t L_r(j)}. \quad (18)$$

The denominator is the normalization over *all* hypotheses. Equivalently, for any fixed k ,

$$\sum_{j=1}^K (\mathbf{p}_0)_j \prod_{r=1}^t L_r(j) = (\mathbf{p}_0)_k \prod_{r=1}^t L_r(k) + \sum_{j \neq k} (\mathbf{p}_0)_j \prod_{r=1}^t L_r(j). \quad (19)$$

H.2.2. STEPWISE BAYES UPDATE

The expression (16) is a “batch” update using the entire likelihood up to time t . Equivalently, we can update *step-by-step* by incorporating the new observation x_t on top of the history $H_t := \{(a_1, x_1), \dots, (a_t, x_t)\}$, so by Bayes' rule,

$$\Pr(z = k \mid H_t) = \frac{p(x_t \mid H_{t-1}, a_t, z = k) \Pr(z = k \mid H_{t-1})}{p(x_t \mid H_{t-1}, a_t)}. \quad (20)$$

Under conditional independence, the past does not affect the distribution of the new observation once we condition on the current action and z :

$$p(x_t \mid a_{1:t}, x_{1:t-1}, z = k) = p(x_t \mid a_t, z = k) =: L_t(k). \quad (21)$$

Moreover, since z is static and choices are treated as exogenous (i.e. we condition on $a_{1:t}$ as given), the belief about z before observing x_t is just the previous posterior:

$$\Pr(z = k \mid a_{1:t}, x_{1:t-1}) = \Pr(z = k \mid a_{1:t-1}, x_{1:t-1}) = p_{t-1}(k). \quad (22)$$

Using the law of total probability and the chain rule $p(A, B \mid C) = p(A \mid B, C) p(B \mid C)$, we can expand as

$$\begin{aligned} p(x_t \mid a_{1:t}, x_{1:t-1}) &= \sum_{j=1}^K p(x_t, z = j \mid a_{1:t}, x_{1:t-1}) = \sum_{j=1}^K p(x_t \mid a_{1:t}, x_{1:t-1}, z = j) \Pr(z = j \mid a_{1:t}, x_{1:t-1}) \\ &= \sum_{j=1}^K p(x_t \mid a_t, z = j) p_{t-1}(j) \\ &= \sum_{j=1}^K L_t(j) p_{t-1}(j). \end{aligned} \quad (23)$$

Substituting (21), (22), and (23) into (20) gives

$$p_t(k) = \frac{p_{t-1}(k) L_t(k)}{\sum_{j=1}^K p_{t-1}(j) L_t(j)}. \quad (24)$$

Given that the likelihoods of a mismatch with the true latent variable are shared, we can also write down the step-wise integrator with choice a_t as depending on

$$L_t^+ := p(x_t \mid a_t, z = a_t) \quad (25)$$

$$L_t^- := p(x_t \mid a_t, z \neq a_t), \quad (26)$$

which leads to the update equation (24) being rewritten as

$$p_t(a_t) = \frac{p_{t-1}(a_t) L_t^+}{p_{t-1}(a_t) L_t^+ + \sum_{j \neq a_t} p_{t-1}(j) L_t^-}. \quad (27)$$

The definition of L_t^+, L_t^- will come useful later when we derive log-ratio accumulator model.

H.2.3. BAYES UPDATE IN PROBABILITY SPACE

Define the likelihood vector $\mathbf{L}_t \in \mathbf{R}_+^K$ by

$$(\mathbf{L}_t)_k := p(x_t \mid a_t, z = k), \quad (28)$$

so that $(\mathbf{L}_t)_k = L_t(k)$ in (24). Then Bayes' rule is the elementwise update plus renormalization gives us Eq. 1

$$\mathbf{p}_t = \frac{\mathbf{p}_{t-1} \odot \mathbf{L}_t}{\mathbf{1}^\top (\mathbf{p}_{t-1} \odot \mathbf{L}_t)}, \quad (29)$$

where \odot denotes componentwise multiplication.

H.2.4. LOG-INTEGRATOR EQUATION

Define the (unnormalized) log-posterior vector at round t

$$\boldsymbol{\ell}_t := \log \mathbf{p}_0 + \sum_{r=1}^t \log \mathbf{L}_r, \quad \text{equivalently} \quad \boldsymbol{\ell}_t = \boldsymbol{\ell}_{t-1} + \log \mathbf{L}_t. \quad (30)$$

Lemma (softmax invariance to common shifts). For any $\mathbf{v} \in \mathbf{R}^K$ and any $\alpha \in \mathbf{R}$,

$$\sigma(\mathbf{v} + \alpha \mathbf{1}) = \sigma(\mathbf{v}). \quad (31)$$

Proposition 1. Define

$$\sigma(\mathbf{v}) := \frac{\exp(\mathbf{v})}{\mathbf{1}^\top \exp(\mathbf{v})}. \quad (32)$$

Then the Bayesian posterior is

$$\mathbf{p}_t = \sigma(\boldsymbol{\ell}_t). \quad (33)$$

where $\sigma(\cdot)$ is the softmax operator.

Proof. By construction,

$$\exp(\boldsymbol{\ell}_t) = \exp(\log \mathbf{p}_0) \odot \prod_{r=1}^t \exp(\log \mathbf{L}_r) = \mathbf{p}_0 \odot \prod_{r=1}^t \mathbf{L}_r,$$

whose k th component is $p_0(k) \prod_{r=1}^t p(x_r \mid a_r, z = k)$, i.e. Bayes' numerator. Normalizing across k yields (33). \square

H.3. Log-ratio accumulator

In this section we first derive the log-ratio accumulator that allows for step-wise information gathering and then prove that it leads to the **Normative Bayes Integrator** defined in Appendix Section H.2.4.

H.3.1. LOG-RATIO EVIDENCE

Assume binary outcomes $x_t \in \{0, 1\}$. Let

$$R \equiv \{x_t = 1\} \quad G \equiv \{x_t = 0\} \quad (34)$$

Under a Bernoulli likelihood with parameter θ we can write explicitly

$$\Pr(R \mid \theta) = \Pr(x_t = 1 \mid \theta) = \theta, \quad (35)$$

$$\Pr(G \mid \theta) = \Pr(x_t = 0 \mid \theta) = 1 - \theta. \quad (36)$$

We can also define the following equivalences:

$$T : z = a_t \quad (\text{match}), \quad F : z \neq a_t \quad (\text{mismatch}). \quad (37)$$

and assume the Bernoulli rate is α_B under T and α_U under F , with $0 < \alpha_U < \alpha_B < 1$, or more concretely

$$p_H(x) = \text{Ber}(x; \alpha_B), \quad p_L(x) = \text{Ber}(x; \alpha_U). \quad (38)$$

The two outcome-specific log-evidence increments (r, g) are then

$$r := \log \frac{\Pr(R \mid T)}{\Pr(R \mid F)} = \log \frac{\alpha_B}{\alpha_U}, \quad (39)$$

$$g := \log \frac{\Pr(G \mid T)}{\Pr(G \mid F)} = \log \frac{1 - \alpha_B}{1 - \alpha_U}. \quad (40)$$

A single evidence step is the log-likelihood ratio between T and F :

$$\log \frac{p_H(x_t)}{p_L(x_t)} = x_t \quad (41)$$

$$r + (1 - x_t) g, r := \log \frac{\alpha_B}{\alpha_U}, \quad (42)$$

$$g := \log \frac{1 - \alpha_B}{1 - \alpha_U}. \quad (43)$$

With these components we can now write in full the (r, g) **counters** that lead to the accumulator we are looking for, concretely if we let $e_{a_t} \in \mathbf{R}^K$ be the one-hot action vector, $(e_{a_t})_k = \mathbf{I}[k = a_t]$ we can define a vector counts of successes and failures per arm by

$$\mathbf{N}_t^{(1)} := \sum_{r=1}^t x_r e_{a_r}, \quad \mathbf{N}_t^{(0)} := \sum_{r=1}^t (1 - x_r) e_{a_r}, \quad (44)$$

which allows us to reach the accumulator state in closed form as

$$\mathbf{q}_t = \log \mathbf{p}_0 + r \mathbf{N}_t^{(1)} + g \mathbf{N}_t^{(0)}. \quad (45)$$

H.3.2. δ_t EVIDENCE RECURSIVE EQUATION

With the above derivation in mind, we can simplify the integrator equation a bit more so as to make the comparisons between the different formalisms easier. If we recall likelihood terms defined previously in 25,26

$$L_t^+ := p(x_t | a_t, z = a_t), \quad L_t^- := p(x_t | a_t, z \neq a_t) \quad (46)$$

we can see that the likelihood vector satisfies

$$(\mathbf{L}_t)_k = p(x_t | a_t, z = k) = \begin{cases} L_t^+, & k = a_t, \\ L_t^-, & k \neq a_t. \end{cases} \quad (47)$$

This is equivalent to the initial the Bernoulli dependent definition

$$L_t^+ = p_H(x_t) = \alpha_B^{x_t} (1 - \alpha_B)^{1-x_t}, \quad (48)$$

$$L_t^- = p_L(x_t) = \alpha_U^{x_t} (1 - \alpha_U)^{1-x_t}, \quad (49)$$

which implies the equivalence

$$\log \frac{L_t^+}{L_t^-} = x_t \log \frac{\alpha_B}{\alpha_U} + (1 - x_t) \log \frac{1 - \alpha_B}{1 - \alpha_U} = x_t r + (1 - x_t) g. \quad (50)$$

Substituting into (45) yields the likelihood-ratio form

$$\mathbf{q}_t = \log \mathbf{p}_0 + \sum_{r=1}^t \log \frac{L_r^+}{L_r^-} e_{a_r}. \quad (51)$$

Define the scalar log-likelihood ratio (single-step evidence)

$$\delta_t := \log \frac{L_t^+}{L_t^-} = \log \frac{p(x_t | a_t, z = a_t)}{p(x_t | a_t, z \neq a_t)}. \quad (52)$$

Then (51) becomes the simplified accumulator definition

$$\mathbf{q}_t := \log \mathbf{p}_0 + \sum_{r=1}^t \delta_r e_{a_r}, \quad (53)$$

or more simply

$$\mathbf{q}_t = \mathbf{q}_{t-1} + \delta_t e_{a_t}. \quad (54)$$

It is also convenient to write the likelihood vector itself as

$$\mathbf{L}_t = L_t^- \mathbf{1} + (L_t^+ - L_t^-) e_{a_t},$$

and in log space (component-wise)

$$\log \mathbf{L}_t = \log(L_t^-) \mathbf{1} + \delta_t e_{a_t}. \quad (55)$$

H.3.3. RECOVERING THE ORIGINAL LOG-INTEGRATOR

Recall from Section 1 that the unnormalized log-posterior (log-integrator) is $\ell_t = \log \mathbf{p}_0 + \sum_{r=1}^t \log \mathbf{L}_r$ (30). Plugging (55) into this definition gives

$$\ell_t = c_t \mathbf{1} + \mathbf{q}_t, \quad c_t := \sum_{r=1}^t \log(L_r^-). \quad (56)$$

Corollary 2.1 (accumulator posterior is Bayesian). Combining (33), (56), and (31),

$$\mathbf{p}_t = (\ell_t) = \sigma(c_t \mathbf{1} + \mathbf{q}_t) = \sigma(\mathbf{q}_t). \quad (57)$$

H.4. Memory Bayesian Integrator

Up to this point we derived several equivalent representations of the Bayesian posterior: the log-integrator ℓ_t (30), log-ratio accumulator \mathbf{q}_t (54), and their relation $\ell_t = c_t \mathbf{1} + \mathbf{q}_t$ (56). These representations are not unique, because the posterior depends only on *relative* log-beliefs: by Lemma (31),

$$\sigma(\mathbf{v} + \alpha \mathbf{1}) = \sigma(\mathbf{v}) \quad (\alpha \in \mathbf{R}),$$

so any global shift along $\mathbf{1}$ is a non-informative degree of freedom. Concretely, the scalar term $c_t \mathbf{1}$ in (56) carries no information about z and cancels under $\sigma(\cdot)$.

A natural way to remove this invariance is to project log-beliefs onto the $(K - 1)$ -dimensional subspace orthogonal to $\mathbf{1}$. We therefore introduce a *centered* log state \mathbf{h}_t defined as the unique representative of the equivalence class $\ell_t + \text{span}\{\mathbf{1}\}$ with zero mean across components. Concretely,

$$\mathbf{h}_t = \ell_t - \frac{1}{K}(\mathbf{1}^\top \ell_t)\mathbf{1},$$

which can be written compactly as $\mathbf{h}_t = C\ell_t$ for an idempotent centering projection C . Working in centered space has two practical advantages for the modeling that follows: (i) it removes unidentifiable global offsets that would otherwise interact with forgetting parameters, and (ii) under the shared-negative-evidence structure (47), the evidence update becomes a simple state-dependent impulse proportional to the δ_t integrator form. We now can formalize this centering operator and derive the centered (state-dependent) recursion that forms the base model for the memory defined in Section 7.

Considering the *centering* projection as

$$C := I - \frac{1}{K}\mathbf{1}\mathbf{1}^\top, \quad C\mathbf{1} = \mathbf{0}, \quad C^2 = C. \quad (58)$$

Define the centered log state

$$\mathbf{h}_t := C\ell_t. \quad (59)$$

From (30),

$$\mathbf{h}_t = C\ell_t = C(\ell_{t-1} + \log \mathbf{L}_t) = \mathbf{h}_{t-1} + C \log \mathbf{L}_t. \quad (60)$$

H.4.1. EQUIVALENCE WITH THE ACCUMULATOR \mathbf{q}_t

Using (55) and $C\mathbf{1} = \mathbf{0}$,

$$C \log \mathbf{L}_t = C(\log(L_t^-)\mathbf{1} + \delta_t e_{a_t}) = \delta_t C e_{a_t} = \delta_t \left(e_{a_t} - \frac{1}{K}\mathbf{1} \right). \quad (61)$$

Therefore the centered (state-dependent) integrator is

$$\mathbf{h}_t = \mathbf{h}_{t-1} + \delta_t \left(e_{a_t} - \frac{1}{K}\mathbf{1} \right). \quad (62)$$

From (56) and $C\mathbf{1} = \mathbf{0}$,

$$\mathbf{h}_t = C\ell_t = C(c_t \mathbf{1} + \mathbf{q}_t) = C\mathbf{q}_t. \quad (63)$$

So \mathbf{h}_t is exactly the *centered version* of the accumulator.

Conversely, because $\text{null}(C) = \text{span}\{\mathbf{1}\}$, \mathbf{h}_t determines \mathbf{q}_t only up to a common shift:

$$\mathbf{h}_t = C\mathbf{q}_t \iff \exists \alpha_t \in \mathbf{R} : \mathbf{q}_t = \mathbf{h}_t + \alpha_t \mathbf{1}. \quad (64)$$

Using (57), (64), and (31),

$$\mathbf{p}_t = \sigma(\mathbf{q}_t) = \sigma(\mathbf{h}_t + \alpha_t \mathbf{1}) = \sigma(\mathbf{h}_t). \quad (65)$$

Since $C\mathbf{q}_t = \mathbf{h}_t$ and $\text{null}(C) = \text{span}\{\mathbf{1}\}$, we have $\mathbf{q}_t = \mathbf{h}_t + \alpha_t \mathbf{1}$ for some scalar α_t . Choosing the canonical representative induced by C (mean-zero \mathbf{h}_t) gives

$$\alpha_t = \frac{1}{K} \mathbf{1}^\top \mathbf{q}_t. \quad (66)$$

Using the accumulator form $\mathbf{q}_t = \log \mathbf{p}_0 + \sum_{r=1}^t \delta_r e_{a_r}$ and $\mathbf{1}_{a_r}^\top = 1$,

$$\alpha_t = \frac{1}{K} \mathbf{1}^\top \log \mathbf{p}_0 + \frac{1}{K} \sum_{r=1}^t \delta_r, \quad (67)$$

$$\alpha_t = \alpha_{t-1} + \frac{\delta_t}{K}. \quad (68)$$

$\alpha_t \mathbf{1}$ is a common shift applied to all coordinates of \mathbf{q}_t and therefore carries no information about relative odds; it is removed by centering and cancels under σ (31). Hence \mathbf{h}_t differs from \mathbf{q}_t (and ℓ_t) only by an additive term in $\text{span}\{\mathbf{1}\}$: it retains exactly the evidence that changes the posterior, while discarding a global baseline drift that does not affect \mathbf{p}_t .

We can thus show that, under the shared-negative-evidence assumption (47),

$$\mathbf{p}_t = \sigma(\ell_t) = \sigma(\mathbf{q}_t) = \sigma(\mathbf{h}_t) \quad (69)$$

where

$$\mathbf{q}_t = \mathbf{q}_{t-1} + \delta_t e_{a_t}, \quad \mathbf{h}_t = \mathbf{h}_{t-1} + \delta_t \left(e_{a_t} - \frac{1}{K} \mathbf{1} \right).$$

Thus starting from the accumulator or starting from the centered integrator yields the same Bayesian posterior.

H.4.2. EVIDENCE INCREMENTS IN CENTERED LOG SPACE

Within game g , the latent target $z \in \{1, \dots, K\}$ is fixed and the agent produces a sequence of choices and outcomes $H_g := (a_{g,1}, x_{g,1}), \dots, (a_{g,t}, x_{g,t})$. All belief states and policies below are defined per game. For a given game and round t , define the likelihood vector exactly as in Section 2:

$$(\mathbf{L}_t)_k := p(x_t \mid a_t, z_n = k), \quad \mathbf{L}_t \in \mathbf{R}_+^K. \quad (70)$$

Define the Bayes-centered log state $\mathbf{h}_t := C\ell_t$ as in (59), and its increment

$$\Delta \mathbf{h}_t := \mathbf{h}_t - \mathbf{h}_{t-1}. \quad (71)$$

From the centered recursion (60), this increment is just the centered log-likelihood:

$$\Delta \mathbf{h}_t = C \log \mathbf{L}_t. \quad (72)$$

Under the shared-negative-evidence structure (47), introduce the match/mismatch likelihoods (identical to (25)–(26) but with indices t)

$$L_t^+ := p(x_t \mid a_t, z = a_t), \quad (73)$$

$$L_t^- := p(x_t \mid a_t, z \neq a_t), \quad (74)$$

and the single-step log-likelihood ratio (LLR) (52)

$$\delta_t := \log \frac{L_t^+}{L_t^-} = \log \frac{p(x_t \mid a_t, z = a_t)}{p(x_t \mid a_t, z \neq a_t)}. \quad (75)$$

Then the decomposition (55) together with $C\mathbf{1} = \mathbf{0}$ implies that the increment in centered space depends *only* on the discriminative LLR term:

$$\Delta \mathbf{h}_t = \delta_t C e_{a_t} = \delta_t \left(e_{a_t} - \frac{1}{K} \mathbf{1} \right). \quad (76)$$

This is exactly the game-indexed version of the centered update (61).

H.4.3. MEMORY STATE UPDATE

The exact Bayesian centered state satisfies $\mathbf{h}_t = \mathbf{h}_{t-1} + \Delta\mathbf{h}_t$. To model forgetting, we replace this perfect accumulation by a recursion on an internal state $\mathbf{h}_t \in \mathbf{R}^K$:

$$\mathbf{h}_0 := C \log \mathbf{p}_0, \quad (77)$$

$$\mathbf{h}_t := (1 - \beta) \mathbf{h}_{t-1} + \Delta\mathbf{h}_t, \quad (78)$$

with $t = \{1, \dots, T\}$, $\beta \in [0, 1]$. Here β controls memory decay: $\beta = 0$ recovers the exact Bayesian centered integrator (because then $\mathbf{h}_t = \mathbf{h}_t$), while larger β discounts older evidence more strongly. Since both $\mathbf{h}_{n,0}$ and $\Delta\mathbf{h}_t$ lie in the centered subspace (orthogonal to $\mathbf{1}$), \mathbf{h}_t remains centered for all t .

The internal posterior used for decision-making is the softmax map applied to the memory state:

$$\bar{\mathbf{p}}_t := \sigma(\mathbf{h}_t). \quad (79)$$

When $\beta = 0$, this coincides with the Bayesian posterior \mathbf{p}_t (cf. (65)).

This same update can be also written as an exponential kernel $\rho := 1 - \beta \in [0, 1]$ where by unrolling (78) yields the causal exponential-kernel representation

$$\mathbf{h}_t = \rho^t \mathbf{h}_0 + \sum_{r=1}^t \rho^{t-r} \Delta\mathbf{h}_r. \quad (80)$$

H.5. Internal posterior and Policy

Following bounded-rationality formulations with information-processing costs (Ortega and Braun, 2013), we model choice as a Gibbs/Boltzmann policy

$$\pi_x(j) \propto \pi_{0,x}(j) \exp(\kappa_x U_x(j)), \quad \pi_x(j) = \frac{1}{Z_x} \pi_{0,x}(j) \exp(\kappa_x U_x(j)), \quad (81)$$

where $\pi_{0,x}$ is a reference (prior) policy, U_x is a utility, and κ_x is an inverse-temperature controlling the strength of exploitation (random as $\kappa_x \rightarrow 0$, increasingly greedy as κ_x grows).

H.5.1. INTERNAL POSTERIOR

In our setting, the memory state \mathbf{h}_t is a centered log-belief (defined up to an additive constant). We choose the bounded-rational utility to be the log-belief coordinate itself,

$$U_x(j) := (\mathbf{h}_{\tau_x(t)})_j, \quad (82)$$

so that evidence accumulated in \mathbf{h} directly determines action values. With a uniform reference policy, (81) yields the *internal posterior*

$$\bar{\mathbf{p}}_t^x := \sigma(\kappa_x \mathbf{h}_{\tau_x(t)}) = \frac{\exp(\kappa_x \mathbf{h}_{\tau_x(t)})}{\mathbf{1}^\top \exp(\kappa_x \mathbf{h}_{\tau_x(t)})} \in \Delta^K, \quad (83)$$

which is equivalent to $\bar{\mathbf{p}}_t^x = \sigma(\kappa_x \mathbf{h}_t)$ (up to the phase/time index $\tau_x(t)$). This makes clear that κ_x interpolates between near-uniform behavior ($\kappa_x \rightarrow 0$), posterior-proportional behavior ($\kappa_x = 1$), and MAP-like concentration as $\kappa_x \rightarrow \infty$. (Equivalently, since $\sigma(\mathbf{h}) \propto \exp(\mathbf{h})$, (83) is identical to raising $\sigma(\mathbf{h}_{\tau_x(t)})$ to a power and renormalizing.)

H.5.2. OCCLUSION MASK

During sampling, not all actions are available: let $\mathcal{A}_{g,t} \subseteq \{1, \dots, K\}$ denote the set of visible (valid) buttons at round t in game g . We encode availability by a multiplicative mask $\mathbf{m}_{g,t}^s \in \mathbb{R}_{>0}^K$ with entries

$$m_{g,t,j}^s := \theta_{\text{occ}}^{-1 \{j \notin \mathcal{A}_{g,t}\}}, \quad j \in \{1, \dots, K\}, \quad (84)$$

so visible actions have weight 1 and occluded actions are down-weighted by $1/\theta_{\text{occ}}$. Larger θ_{occ} therefore corresponds to stronger occlusion awareness (greater avoidance of invalid actions). At the final decision round, all actions are available and we set $\mathbf{m}_{g,t}^f \equiv \mathbf{1}$.

Bias and policy. We incorporate systematic preferences and availability constraints through a phase-specific reference policy $\pi_{0,x}(j) \propto \omega_x(j) m_t^x(j)$, where $\omega_x \in \Delta^K$ is a choice-bias vector and m_t^x is an occlusion mask (with $m_t^f \equiv \mathbf{1}$). Combining (81) and (83) yields the full policy

$$\pi_t^x = \frac{\bar{\mathbf{p}}_t^x \odot \omega_x \odot \mathbf{m}_t^x}{\mathbf{1}^\top (\bar{\mathbf{p}}_t^x \odot \omega_x \odot \mathbf{m}_t^x)}. \quad (85)$$

H.6. Model loss function

For each agent (human or LLM condition), the dataset consists of G games. Game g provides sampling choices $\{a_{g,t}\}_{t=1}^{T_g}$, observed outcomes $\{x_{g,t}\}_{t=1}^{T_g}$, occlusion sets $\{\mathcal{A}_{g,t}\}_{t=1}^{T_g}$ (sampling only), and a final inference choice f_g . Given parameters

$$\Theta := (\omega_s, \omega_f, \kappa_s, \kappa_f, \beta, \theta), \quad (86)$$

we *unroll* the memory trajectory $\{\mathbf{h}_{g,t}\}$ deterministically from the observed history using the memory update (Eq. (4)) and the corresponding evidence injection $\Delta \mathbf{h}_{g,t}$. At each sampling round t we compute the internal posterior $\bar{\mathbf{p}}_{g,t}^s$ from the pre-observation state $\mathbf{h}_{g,t-1}$ (Eq. (83)) and form the sampling policy $\pi_{g,t}^s$ via Eq. (85) using the occlusion mask $\mathbf{m}_{g,t}^s$ (derived from $\mathcal{A}_{g,t}$ and θ). After the last update, we compute the final policy π_g^f from \mathbf{h}_{g,T_g} with $\mathbf{m}^f \equiv \mathbf{1}$.

The conditional log-likelihood of the observed choices under the induced policies is

$$\mathcal{L}(\Theta) = \sum_{g=1}^G \left[\sum_{t=1}^{T_g} \log (\pi_{g,t}^s)_{a_{g,t}} + \log (\pi_g^f)_{f_g} \right] + \Omega(\Theta) \quad (87)$$

and we estimate Θ by minimizing a regularized negative log-likelihood (Daw, 2011; Bishop, 2006) with a simple quadratic regularizer (one choice among many)

$$\Omega(\Theta) = \lambda_\omega \sum_{x \in \{s, f\}} \left\| \omega_x - \frac{1}{K} \mathbf{1} \right\|_2^2 + \lambda_\kappa (\kappa_s^2 + \kappa_f^2) + \lambda_\beta (\beta - \beta_0)^2 + \lambda_{\text{occ}} (\log \theta_{\text{occ}})^2, \quad (88)$$

where $\lambda_\omega, \lambda_\kappa, \lambda_\beta, \lambda_{\text{occ}} \geq 0$ and β_0 is a chosen reference value.

I. Fitting Results

For each agent (humans and each LLM) and reasoning mode (*Base/Extended*), Appendix Figs. 9–12 visualize (i) posterior trajectories during *inference* and *sampling*, and (ii) choice biases alongside the fitted bias weights $\{\omega_s, \omega_f\}$. The same quantities are summarized as heatmaps in Appendix Fig. 13. Full fitted parameter values are reported in Table J (corresponding to Fig. 3 in the main text).

Posterior curves. All posterior panels compress the full K -dimensional belief vector into a single scalar by reading out the posterior mass assigned to the choice that was actually taken. Concretely, let $\mathbf{p}_{g,t} \in \Delta^K$ denote the (normative) Bayesian posterior after t samples in game g . Then for *inference* panels (columns 1–2), the plotted quantity is the posterior probability of the *final chosen option*, evaluated as evidence accumulates across rounds. While for *sampling* panels (columns 3–4), the plotted quantity is the posterior probability of the *sampling action chosen on round t* , evaluated *just before* the sample is taken on that round (so that it reflects the beliefs that informed the sampling decision).

Curves are grouped by trial length $N \in \{2, \dots, 15\}$. For a fixed N , we compute the scalar trajectory above for every game of length N and then average across games, producing one mean trajectory per N (shown as a family of curves, ordered by N). Thus, each line summarizes the *average posterior dynamics conditional on game length* for *inference* and *sampling*.

True posteriors are computed from the observed trajectories of each agent, and **fitted posteriors** from trajectories simulated by the fitted model, in both cases using the same normative Bayesian update (Eq. 1).

Bias panels. The bias panels compare empirical choice frequencies against the fitted bias weights. Empirical bars report how often each option is chosen (separately for sampling and inference), while the fitted bars show the learned bias vectors ω_s and ω_f (or their summary statistic, depending on the plot), which capture systematic preferences not explained by the posterior.

Important note. The “fitted posterior” curves are *not* directly optimized by the likelihood. They are emergent summaries obtained by running the fitted model, collecting its actions, and then reconstructing the same posterior-readout trajectories from those actions (analogous to the empirical construction).

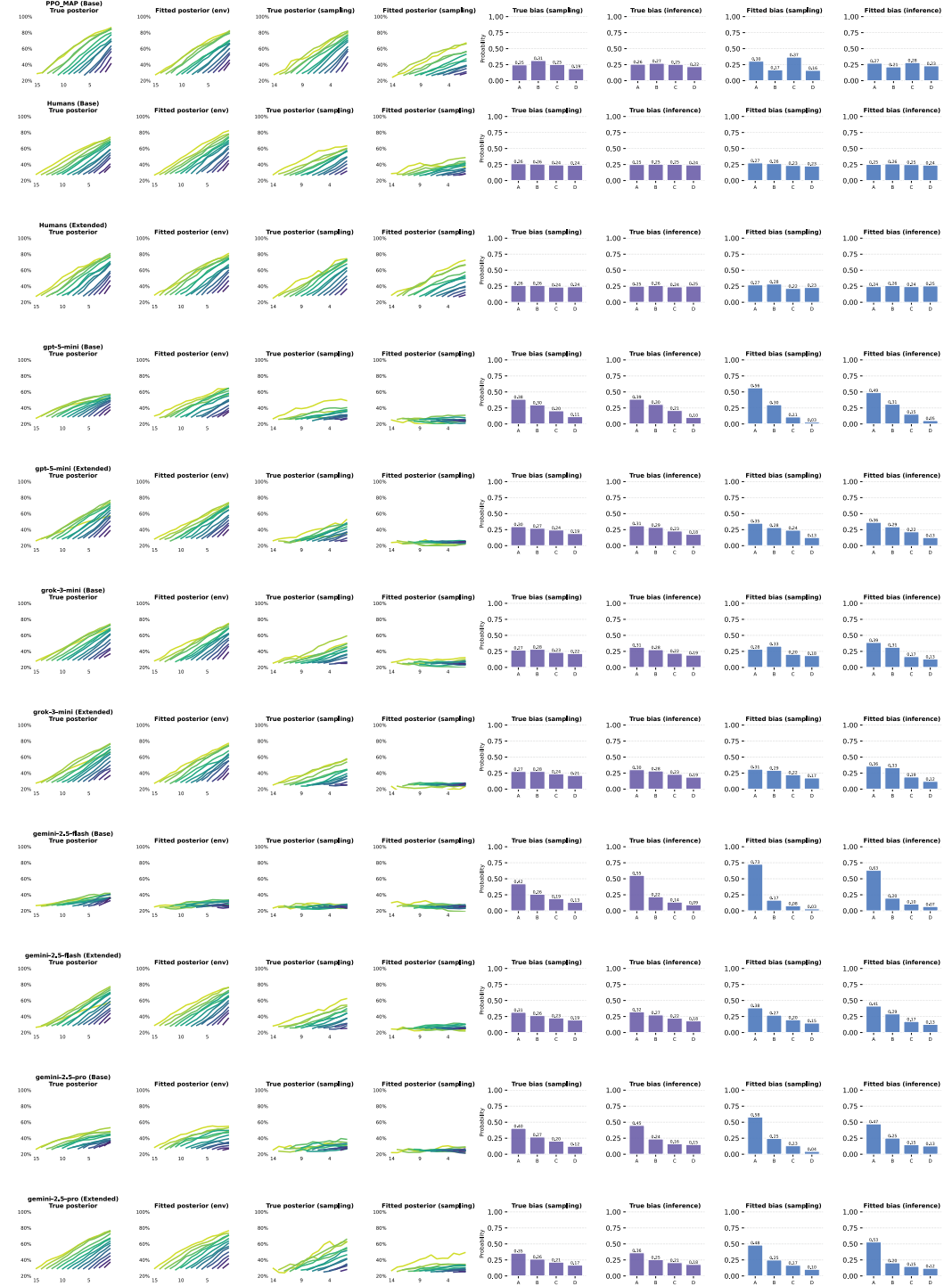


Figure 9. Posterior evolution by rounds and bias across humans and language models. In each row the first two panels represent the true and model generated posterior evolution of the final choice *inference* followed by the true and model generated posterior for the sampling choices *sampling*. The remaining panels show the true bias for sampling and inference and their corresponding fitted bias weights.

Reasoning aligns language models to human cognition

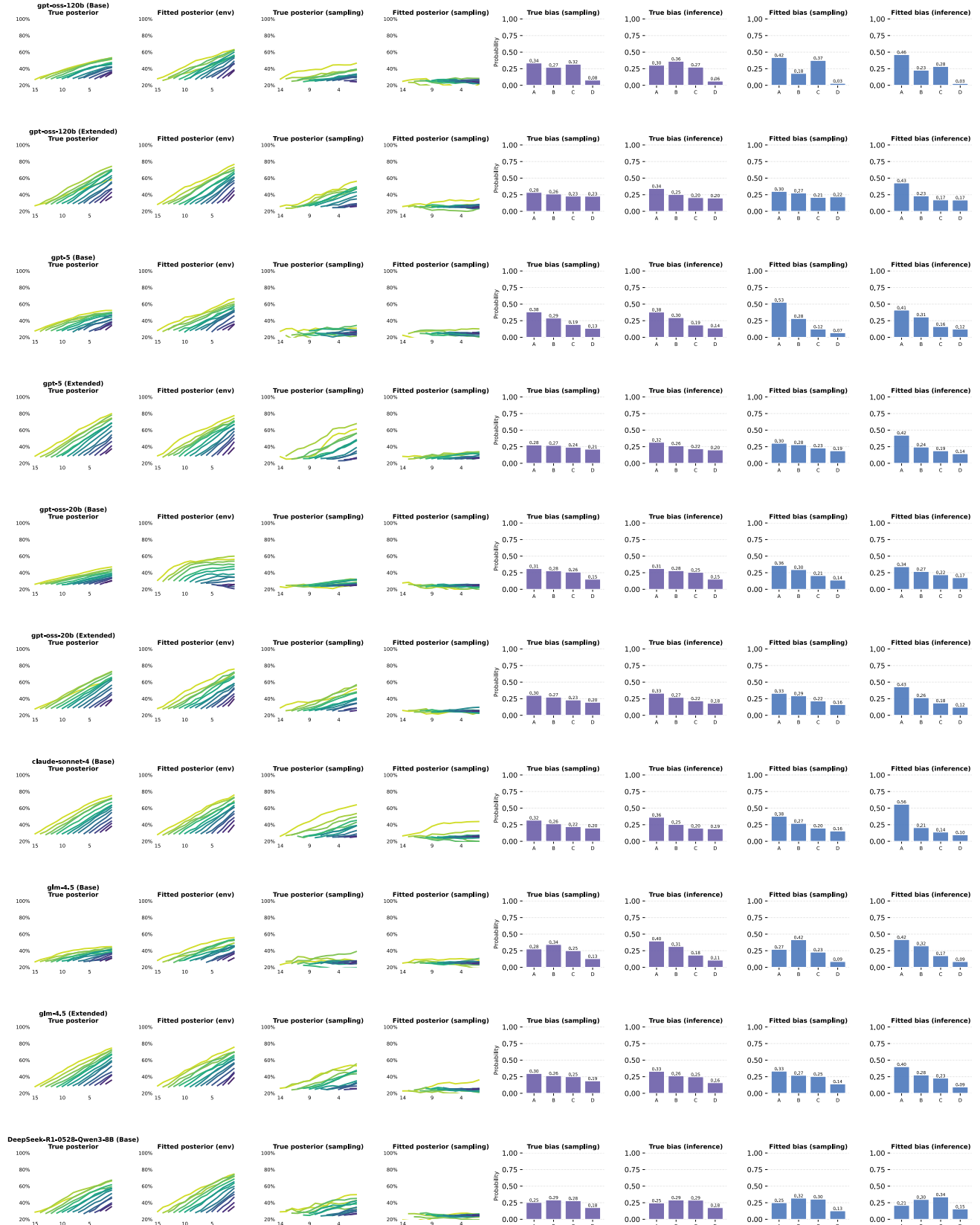


Figure 10. Posterior evolution by rounds and bias across humans and language models. In each row the first two panels represent the true and model generated posterior evolution of the final choice *inference* followed by the true and model generated posterior for the sampling choices *sampling*. The remaining panels show the true bias for sampling and inference and their corresponding fitted bias weights.

Reasoning aligns language models to human cognition

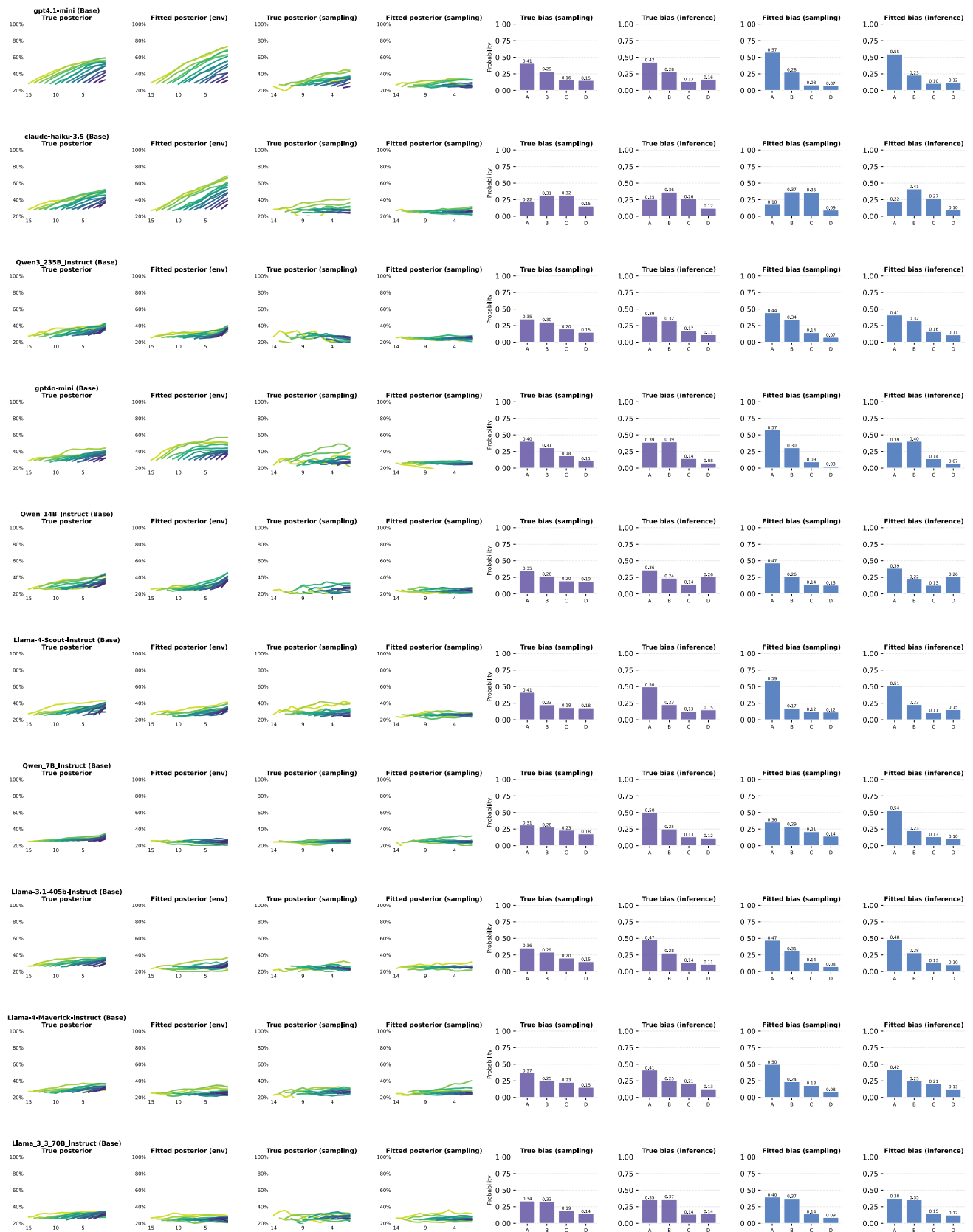


Figure 11. Posterior evolution by rounds and bias across humans and language models. In each row the first two panels represent the true and model generated posterior evolution of the final choice *inference* followed by the true and model generated posterior for the sampling choices *sampling*. The remaining panels show the true bias for sampling and inference and their corresponding fitted bias weights.

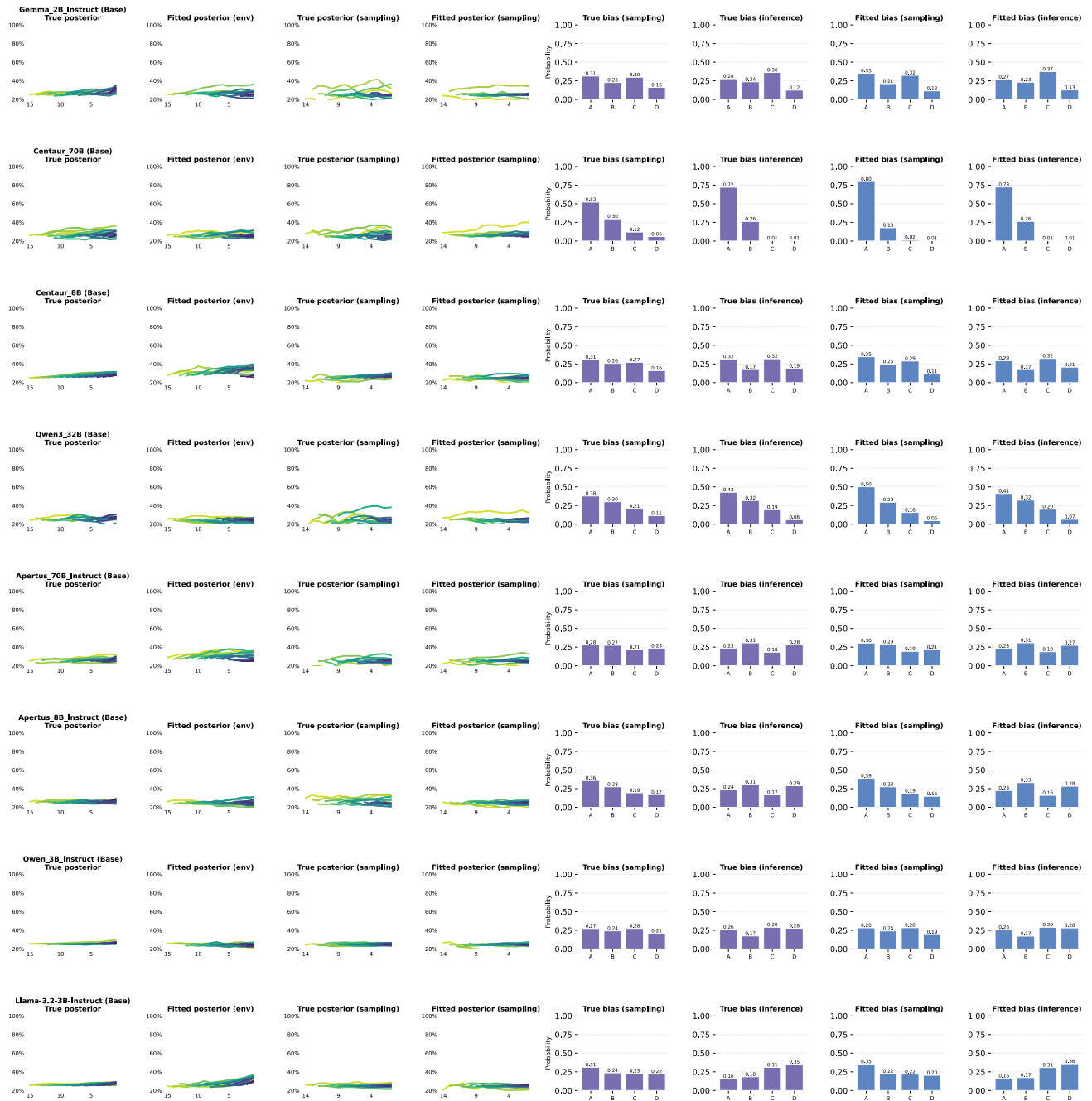


Figure 12. Posterior evolution by rounds and bias across humans and language models. In each row the first two panels represent the true and model generated posterior evolution of the final choice *inference* followed by the true and model generated posterior for the sampling choices *sampling*. The remaining panels show the true bias for sampling and inference and their corresponding fitted bias weights.

Reasoning aligns language models to human cognition

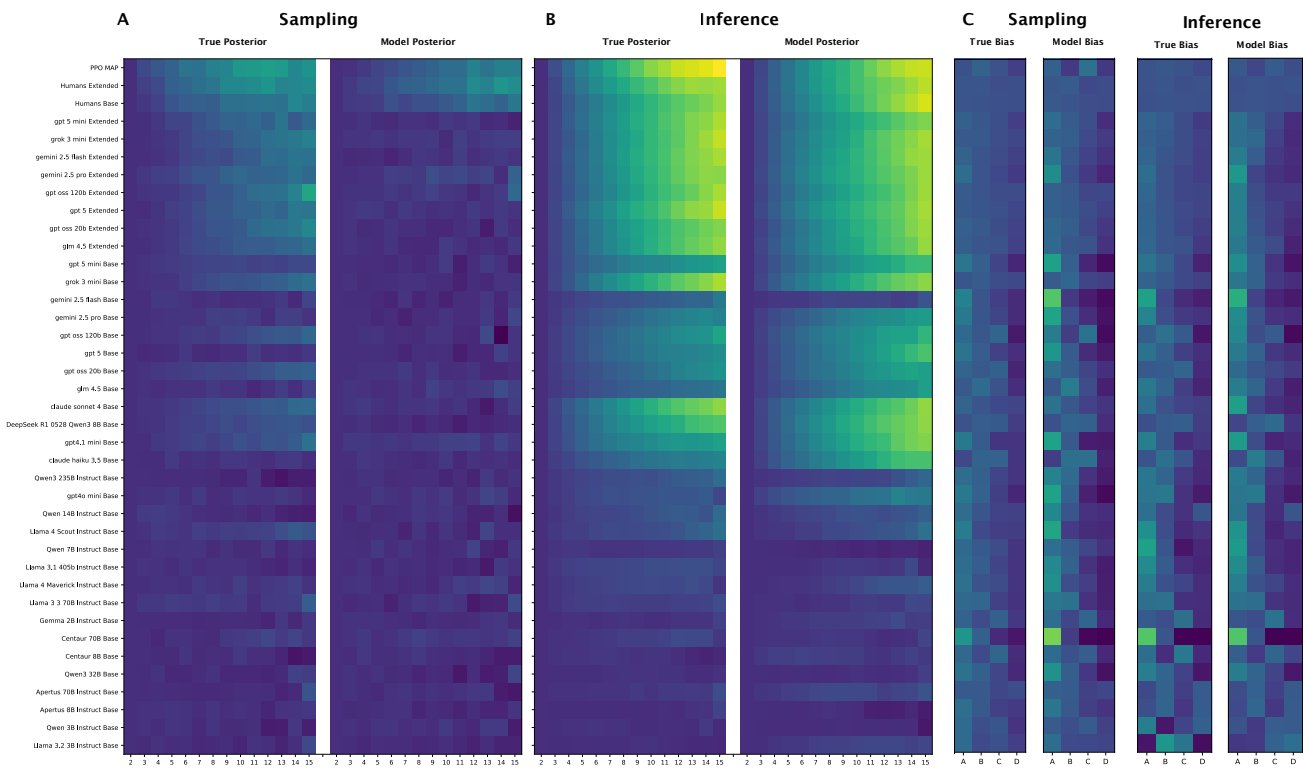


Figure 13. Posterior and bias structure is captured by the mechanistic model. For each agent (rows), we compute phase-specific summaries during **sampling** (left block) and **inference** (middle block), and compare empirical estimates (**True**) to quantities generated by the fitted mechanistic model (**Model**). **Sampling:** heatmaps show the agent’s **True Posterior** signal (normative posterior mass assigned to the agent’s eventual choice under the game history) alongside the corresponding **Model Posterior** obtained by unrolling the fitted belief dynamics. **Inference:** analogous comparison for the final inference phase. **Bias:** right block contrasts **True Bias** (empirical action preference beyond belief) with **Model Bias** recovered from the multiplicative bias parameters. Across agents, the model reproduces both the magnitude and qualitative structure of posterior dynamics and systematic biases, supporting the claim that $(\beta, \kappa, \omega, \theta)$ provide a sufficient explanation of the behavioral signatures.

J. Model Fitting Parameters

Table 1. Fitted parameters of the model

Model	Reasoning	ω_s	ω_f	β	κ_s	κ_f	$\log \theta$
PPO MAP	Base	[0.304, 0.168, 0.367, 0.161]	[0.273, 0.215, 0.282, 0.231]	-0.016	0.607	9.971	7.449
Humans	Base	[0.275, 0.264, 0.235, 0.227]	[0.251, 0.259, 0.249, 0.240]	-0.028	0.378	1.179	6.977
Humans	Extended	[0.271, 0.284, 0.215, 0.230]	[0.243, 0.259, 0.243, 0.254]	-0.061	0.616	1.697	7.166
gpt-5-mini	Base	[0.564, 0.300, 0.109, 0.028]	[0.489, 0.308, 0.152, 0.052]	-0.036	0.000	0.706	2.336
gpt-5-mini	Extended	[0.350, 0.283, 0.241, 0.127]	[0.363, 0.294, 0.216, 0.126]	0.043	0.000	2.249	3.226
grok-3-mini	Base	[0.283, 0.330, 0.203, 0.183]	[0.388, 0.314, 0.168, 0.130]	0.014	0.000	1.971	3.668
grok-3-mini	Extended	[0.310, 0.293, 0.224, 0.173]	[0.358, 0.333, 0.188, 0.121]	0.002	0.063	2.147	4.153
gemini-2.5-flash	Base	[0.727, 0.165, 0.078, 0.030]	[0.632, 0.197, 0.105, 0.066]	0.140	0.000	0.357	3.672
gemini-2.5-flash	Extended	[0.384, 0.270, 0.199, 0.147]	[0.412, 0.290, 0.172, 0.127]	0.003	0.046	1.755	3.344
gemini-2.5-pro	Base	[0.580, 0.245, 0.132, 0.043]	[0.473, 0.251, 0.148, 0.128]	-0.032	0.000	0.228	7.261
gemini-2.5-pro	Extended	[0.482, 0.248, 0.167, 0.103]	[0.530, 0.203, 0.148, 0.119]	-0.063	0.121	1.377	6.788
gpt-oss-120b	Base	[0.418, 0.179, 0.375, 0.029]	[0.462, 0.227, 0.283, 0.027]	0.047	0.000	0.983	1.197
gpt-oss-120b	Extended	[0.299, 0.275, 0.209, 0.217]	[0.427, 0.232, 0.171, 0.170]	0.004	0.041	1.660	1.827
gpt-5	Base	[0.526, 0.283, 0.123, 0.068]	[0.410, 0.306, 0.162, 0.123]	0.044	0.000	0.565	2.024
gpt-5	Extended	[0.302, 0.279, 0.231, 0.188]	[0.423, 0.244, 0.188, 0.144]	-0.036	0.081	2.336	6.828
gpt-oss-20b	Base	[0.359, 0.296, 0.206, 0.139]	[0.340, 0.268, 0.218, 0.174]	-0.401	0.000	0.026	1.222
gpt-oss-20b	Extended	[0.331, 0.293, 0.216, 0.160]	[0.429, 0.265, 0.185, 0.122]	0.020	0.000	1.821	1.429
claude-sonnet-4	Base	[0.377, 0.270, 0.199, 0.155]	[0.558, 0.205, 0.139, 0.098]	-0.013	0.000	2.413	3.696
glm-4.5	Base	[0.270, 0.415, 0.228, 0.086]	[0.418, 0.323, 0.174, 0.085]	0.028	0.000	0.287	1.595
glm-4.5	Extended	[0.334, 0.270, 0.254, 0.142]	[0.401, 0.276, 0.228, 0.095]	-0.013	0.010	1.988	2.685
DeepSeek-R1-Qwen3-8B	Base	[0.250, 0.319, 0.304, 0.127]	[0.210, 0.298, 0.337, 0.155]	-0.004	0.000	0.787	2.202
gpt4.1-mini	Base	[0.575, 0.276, 0.081, 0.069]	[0.548, 0.230, 0.104, 0.119]	-0.044	0.039	0.697	2.080
claude-haiku-3.5	Base	[0.179, 0.366, 0.362, 0.093]	[0.224, 0.412, 0.269, 0.095]	0.039	0.000	0.618	2.333
Qwen3 235B Instruct	Base	[0.444, 0.340, 0.143, 0.073]	[0.410, 0.322, 0.158, 0.110]	0.673	0.000	1.572	3.506
gpt4o-mini	Base	[0.574, 0.305, 0.094, 0.027]	[0.390, 0.403, 0.139, 0.068]	-0.438	0.011	0.043	3.419
Qwen 14B Instruct	Base	[0.466, 0.261, 0.141, 0.132]	[0.386, 0.223, 0.130, 0.261]	0.492	0.000	1.126	3.773
Llama-4-Scout-Instruct	Base	[0.588, 0.174, 0.123, 0.116]	[0.512, 0.228, 0.107, 0.152]	0.404	0.000	0.738	1.967
Qwen 7B Instruct	Base	[0.356, 0.290, 0.211, 0.143]	[0.535, 0.225, 0.135, 0.105]	0.316	0.000	0.316	1.555
Llama-3.1-405b-Instruct	Base	[0.472, 0.309, 0.143, 0.076]	[0.481, 0.282, 0.132, 0.104]	0.912	0.000	0.408	3.435
Llama-4-Maverick-Instruct	Base	[0.498, 0.237, 0.181, 0.084]	[0.419, 0.248, 0.206, 0.126]	1.000	0.000	0.206	2.152
Llama 3 3 70B Instruct	Base	[0.396, 0.374, 0.142, 0.088]	[0.376, 0.354, 0.146, 0.123]	0.971	0.000	0.000	1.824
Gemma 2B Instruct	Base	[0.351, 0.212, 0.323, 0.115]	[0.268, 0.231, 0.374, 0.128]	0.009	0.000	0.060	1.756
Centaur 70B	Base	[0.799, 0.179, 0.018, 0.005]	[0.726, 0.264, 0.005, 0.005]	0.992	0.000	0.000	2.420
Centaur 8B	Base	[0.346, 0.250, 0.289, 0.115]	[0.294, 0.175, 0.324, 0.207]	-1.000	0.003	0.016	2.349
Qwen3 32B	Base	[0.502, 0.295, 0.157, 0.047]	[0.412, 0.322, 0.201, 0.065]	0.996	0.000	0.000	2.435
Apertus 70B Instruct	Base	[0.304, 0.289, 0.193, 0.214]	[0.231, 0.307, 0.188, 0.274]	-0.939	0.000	0.006	1.752
Apertus 8B Instruct	Base	[0.389, 0.275, 0.187, 0.149]	[0.225, 0.331, 0.161, 0.283]	0.999	0.000	0.000	0.948
Qwen 3B Instruct	Base	[0.283, 0.241, 0.284, 0.192]	[0.256, 0.172, 0.290, 0.282]	-0.317	0.000	0.000	0.879
Llama-3.2-3B-Instruct	Base	[0.353, 0.224, 0.219, 0.203]	[0.162, 0.172, 0.308, 0.358]	0.279	0.000	0.253	1.330
Gemma 2B	Base	[0.284, 0.379, 0.272, 0.065]	[0.334, 0.337, 0.242, 0.087]	0.993	0.000	0.000	0.603
Llama-3.1-8B-Instruct	Base	[0.921, 0.048, 0.026, 0.005]	[0.754, 0.107, 0.110, 0.029]	0.985	0.000	0.000	2.302

Table 2. Negative log-likelihoods of the mechanistic model fitsnot .

Model	Reasoning	Train NLL	Test NLL	NLL
PPO MAP	Base	0.576	0.580	0.580
Humans	Base	0.724	0.724	0.724
Humans	Extended	0.627	0.630	0.630
gpt-5-mini	Base	0.540	0.569	0.569
gpt-5-mini	Extended	0.593	0.634	0.634
grok-3-mini	Base	0.605	0.605	0.605
grok-3-mini	Extended	0.641	0.631	0.631
gemini-2.5-flash	Base	0.466	0.495	0.495
gemini-2.5-flash	Extended	0.613	0.612	0.612
gemini-2.5-pro	Base	0.534	0.518	0.518
gemini-2.5-pro	Extended	0.551	0.574	0.574
gpt-oss-120b	Base	0.869	0.874	0.874
gpt-oss-120b	Extended	0.737	0.734	0.734
gpt-5	Base	0.651	0.676	0.676
gpt-5	Extended	0.586	0.592	0.592
gpt-oss-20b	Base	0.976	0.960	0.960
gpt-oss-20b	Extended	0.825	0.833	0.833
claude-sonnet-4	Base	0.583	0.583	0.583
glm-4.5	Base	0.845	0.849	0.849
glm-4.5	Extended	0.779	0.786	0.786
DeepSeek-R1-0528-Qwen3-8B	Base	0.765	0.772	0.772
gpt4.1-mini	Base	0.595	0.600	0.600
claude-haiku-3.5	Base	0.657	0.679	0.679
Qwen3 235B Instruct	Base	0.585	0.602	0.602
gpt4o-mini	Base	0.495	0.444	0.444
Qwen 14B Instruct	Base	0.625	0.642	0.642
Llama-4-Scout-Instruct	Base	0.728	0.759	0.759
Qwen 7B Instruct	Base	0.825	0.848	0.848
Llama-3.1-405b-Instruct	Base	0.628	0.626	0.626
Llama-4-Maverick-Instruct	Base	0.748	0.742	0.742
Llama 3 3 70B Instruct	Base	0.722	0.723	0.723
Gemma 2B Instruct	Base	0.774	0.799	0.799
Centaur 70B	Base	0.427	0.469	0.469
Centaur 8B	Base	0.726	0.725	0.725
Qwen3 32B	Base	0.607	0.589	0.589
Apertus 70B Instruct	Base	0.804	0.790	0.790
Apertus 8B Instruct	Base	1.045	1.048	1.048
Qwen 3B Instruct	Base	1.113	1.153	1.153
Llama-3.2-3B-Instruct	Base	1.030	1.026	1.026
Gemma 2B	Base	1.171	1.177	1.177
Llama-3.1-8B-Instruct	Base	0.500	0.546	0.546